

# NEAR-SURFACE AND TOPOGRAPHIC DISTORTIONS IN ELECTROMAGNETIC INDUCTION

GEORGE R. JIRACEK

*Department of Geological Sciences, San Diego State University, San Diego, CA 92182, U.S.A.*

**Abstract.** The most revealing description of electromagnetic (EM) distortions due to near-surface inhomogeneities and topography is in terms of galvanic and inductive effects. In either case, the distorted electric and magnetic fields can be best visualized as a vectorial sum of primary and secondary fields. Secondary electric fields due to electric charge build-up in the galvanic case persist to the longest periods. In contrast, the secondary electric and magnetic fields due to inductive, vortex currents disappear at long periods. The static shift of magnetotelluric (MT) apparent resistivity sounding curves is a classic example of the galvanic effect.

Methods to correct for unwanted distortions such as the static shift can be classified into six categories: use of invariant response parameters, curve shifting, statistical averaging, spatial filtering, use of distortion tensors, and computer modeling. Although invariant impedance calculations are simple to make, they cannot, in general, recover the undistorted impedance. Short period curve shifting is best done with auxiliary soundings such as time domain EM; however, this requires multiple surveys. The shifting of long period MT sounding branches is useful if a standard curve is known and can be matched. Statistical averaging of neighboring MT soundings that are conformal but static shifted has proven very effective at removing random distortions if adequate data are available. The new EMAP (Electromagnetic Array Profiling) method combats the inherent spatial high pass characteristics of EM distortions by low pass operations in data collection and processing. EMAP proposes the continuous, in-field measurement of electric field dipoles to avoid spatial aliasing. Distortion tensor stripping of topographic distortions is possible since terrain is deterministic but stripping the effects of uncertain subsurface inhomogeneities may be misleading. A new decomposition of the MT impedance tensor under the assumption of surficial three-dimensional (3-D) galvanic effects imposed on a one- or two-dimensional (1-D and 2-D) regional setting promises a way to recover the regional structure. There is a continual need for 3-D computer modeling to test new methods and to calculate topographic and regional effects. Computer modeling has established the value of 2-D modeling of the data identified as transverse magnetic (TM) in some 3-D environments. Ideally, EM distortion correction requires continuous, or at least many, data and the application of more than one correction-modeling scheme.

## Introduction

The physical principles governing electromagnetic (EM) distortions due to near-surface inhomogeneities and topography have been understood for several decades yet no comprehensive method to correct these distortions has appeared. A very significant description of the problem in magnetotelluric (MT) investigations occurred in the Soviet Union when Berdichevsky *et al.* (1973) (also described in Berdichevsky and Dmitriev, 1976a, 1976b) proposed an approximate, simplified classification of distorted EM fields into inductive and galvanic effects. Jones and Price (1970) also recognized the role of boundary charges (the galvanic effect) in the perturbations of natural EM fields. Even so, the concept of boundary charges is still the source of some skepticism and much discussion amongst EM practitioners; such debate contributed to recent articles on the topic (e.g., Kaufman, 1985; McNeill,

1985). Earlier reviews of the overall EM distortion problem have been given by Jones (1983) and Menvielle (1988). Jones (1983) advocated the principle of "Occam's Razor" whereby, "the simplest of physical models, that describe the observations, must be sought". Menvielle (1988) emphasized simple criteria to recognize the physical phenomena governing EM distortions. He made no distinction between actual topographic effects and surface conductivity heterogeneities. In their introductory remarks of Jones' (1983) review paper, Dosso and Weaver (1983) state that "Doubtless we shall hear more on this subject at future workshops". The same can be said of the present review.

This review mainly treats natural source problems with an emphasis on the MT method. Brief references are made to VLF (very low frequency) and other controlled source techniques. Near-surface inhomogeneities ranging from tiny patches (m scale) to basin-size (tens of km scale) are considered distinct from topographic effects. A review of the underlying physics of the phenomena uses the inductive-galvanic separation. The concept of secondary fields due to boundary charges provides the unifying description of all galvanic effects. Consequently, the common terminologies such as current channeling, flow around effect, etc. and of the deflection of telluric currents by galvanic charges are explained by the vectorial addition of secondary and primary fields. The direct extension of this description to regional-wide current distortions such as the coast, island, and isthmus effects are beyond the scope of this paper. The reader may want to consult the works of, e.g., Nienaber *et al.* (1976), Parkinson and Jones (1979), Honkura *et al.* (1981), Honkura (1983, 1987) or Fischer and Weaver (1986) in this regard.

The present paper endeavors to review most methods currently used to remove near-surface EM distortions. The emphasis is placed on new publications; however, supporting references are made to older works. Overall concepts are stressed and equations are kept to a minimum. Some appraisal and critical comments regarding the various correction schemes are offered. These are not comprehensive nor is there any claim that every correction technique has been addressed. The reader may be disappointed to learn that no magical solution to all problems of near-surface EM distortion is available. However, there may be a method that fits your specific needs or as recently stressed by Berdichevsky *et al.* (1989), a combination of methods is usually required.

### **Physical Characteristics of EM Distortions**

Discussions of the correction techniques proposed to reduce near-surface and topographic distortions in EM measurements must firmly be formulated in terms of the physics of the phenomena. The most practical description of the complex processes has been the classification by Berdichevsky *et al.* (1973) into two major effects, namely galvanic and inductive. As further discussed by Berdichevsky and Dmitriev (1976b), Berdichevsky and Zhdanov (1984), and Zhdanov (1987) these concepts view a 'normal', layered earth response which is distorted. The distortion

is by galvanic excess electric charges together with galvanic and inductive excess currents arising through horizontal deviations from the background layered earth. Distortions to the 'normal' EM fields are termed 'anomalous' fields in the Soviet literature. However, following Hohmann (1988), this review will use the terms primary field for the 'normal' (layered earth) component and secondary fields for the 'anomalous' component of the total fields.

The galvanic effect is caused by the primary electric field producing electric charges where variations in conductivity occur, i.e., at distinct boundaries or at continuous transitions. These excess charges result in secondary electric fields which add vectorially to the primary electric field. The low frequency galvanic secondary electric field is a Coulombian field which can be calculated directly as the gradient of a scalar potential (Menvielle, 1988).

The inductive effect follows Faraday's law, whereby the time derivative of the primary magnetic field induces excessive currents. These vortex currents flowing in closed loops produce secondary magnetic fields which add vectorially to the primary magnetic fields. Secondary electric fields corresponding to self and mutual induction may be expressed as a time derivative of a vector potential (Menvielle, 1988).

The preceding classification is not without some problems, for example, the vortical current induced by secondary magnetic fields associated with the secondary currents in the galvanic effect is an inductive-galvanic effect (Berdichevsky and Zhdanov, 1984). Calculations of these magnetic fields require a volume integration of the excess current density. Still, the classification into galvanic and inductive effects provides enormous practical simplification and insight.

### GALVANIC EFFECTS

As discussed by Rokityansky (1982), the concept of excess charges is really a microscopic view of the situation which is not required if one treats the macroscopic description of current redistribution in inhomogeneous media. Thus, the galvanic effect is known by different terminologies, for example, vertical and horizontal current gathering, current channeling, and current concentration into conductive zones and the flow around effect and current deflection around resistive bodies (e.g., Berdichevsky and Dmitriev, 1967b; Jones, 1983; Park, 1985). The distinction between two- and three-dimensional (2-D and 3-D) inhomogeneities is also made in many definitional terms.

Since it has been clearly demonstrated (e.g., Price, 1973; Kaufman, 1985) that the underlying cause of galvanic electric field (and, therefore, current) redistributions is charge buildup, the microscopic approach is treated here as the unifying description.

Applying the equation of continuity and Ohm's Law, it is easy to show (e.g., Lajoie and West, 1976; Kaufmann, 1985; Pellerin, 1988) that the volume charge density  $\rho_v$  in a material is given by

$$\rho_v = -\frac{\epsilon_0}{\sigma + i\omega\epsilon_0} \mathbf{E} \cdot \nabla\sigma. \quad (1)$$

Here,  $\omega$  is the angular frequency and the dielectric permittivity  $\epsilon_0$  has been taken as a constant; however, the charge density is a function of position since the total electric field  $\mathbf{E}$  and the conductivity  $\sigma$  may vary with  $x$ ,  $y$ , and  $z$ . The key relation here is that if  $\mathbf{E} \cdot \nabla\sigma$  is nonzero, i.e., if there is a component of the electrical field in the direction of a change in conductivity, then charges accumulate. For most geophysical EM methods the quasistatic approximation is appropriate, therefore,  $\sigma \gg \omega\epsilon_0$  and

$$\rho_v \simeq -\frac{\epsilon_0}{\sigma} \mathbf{E} \cdot \nabla\sigma. \quad (2)$$

This shows that there is no temporal phase variation between the changing current and the charge produced under the quasistatic approximation.

Equation (2) indicates that charge may be smeared over a considerable volume of inhomogeneous media having continuous conductivity variations. At sharp conductivity contrasts the volume charge density reduces to a surface charge density  $\rho_s$ . In this case, at a media 0/1 interface with normal field  $E_0^n$ , Equation (2) becomes

$$\rho_s = -\epsilon_0 \frac{\sigma_1 - \sigma_0}{\sigma_1} E_0^n. \quad (3)$$

As pointed out by Price (1973), the surface charge is minute because of the permittivity term, but the secondary electric fields  $\mathbf{E}_s$  can be quite large since, in the low frequency limit, by Coulomb's law

$$\begin{aligned} \mathbf{E}_s &= -\nabla\psi \\ &= -\frac{1}{4\pi\epsilon_0} \int_s \frac{\rho_s}{|\mathbf{r}|^2} \mathbf{r}_0 \, ds. \end{aligned} \quad (4)$$

Here,  $\psi$  is the scalar potential and  $\mathbf{r}$  is a vector between a differential surface element  $ds$  and the observation point;  $\mathbf{r}_0$  is a unit  $\mathbf{r}$  vector.

An understanding of the galvanic concept applied to the EM response of near-surface inhomogeneities and topography can be easily visualized by reference to the sketches in Figure 1. Here, the spatial relationship between the primary electric field  $\mathbf{E}_p$  (assumed uniform), the surface charges, the associated secondary electric field, and the final total current are presented. In Figures 1a and 1b the primary electric field  $\mathbf{E}_p$  is orientated along the major axis of an elliptically-shaped surficial, 3-D inhomogeneity shown in plan view. Figure 1a contains the case of a conductive inclusion and the body is a resistivity one in Figure 1b. Charges form at the boundaries of the body in accordance with Equation (3). The polarity of the charges result in a secondary field opposing the primary field in the conductive body (Figure 1a) and additive to the primary field in the resistive inclusion (Figure 1b). These directions are required to maintain the continuity of current density normal to the boundaries. Upon vectorial addition of the primary field and secondary field configurations shown in Figures 1a and 1b one can estimate the

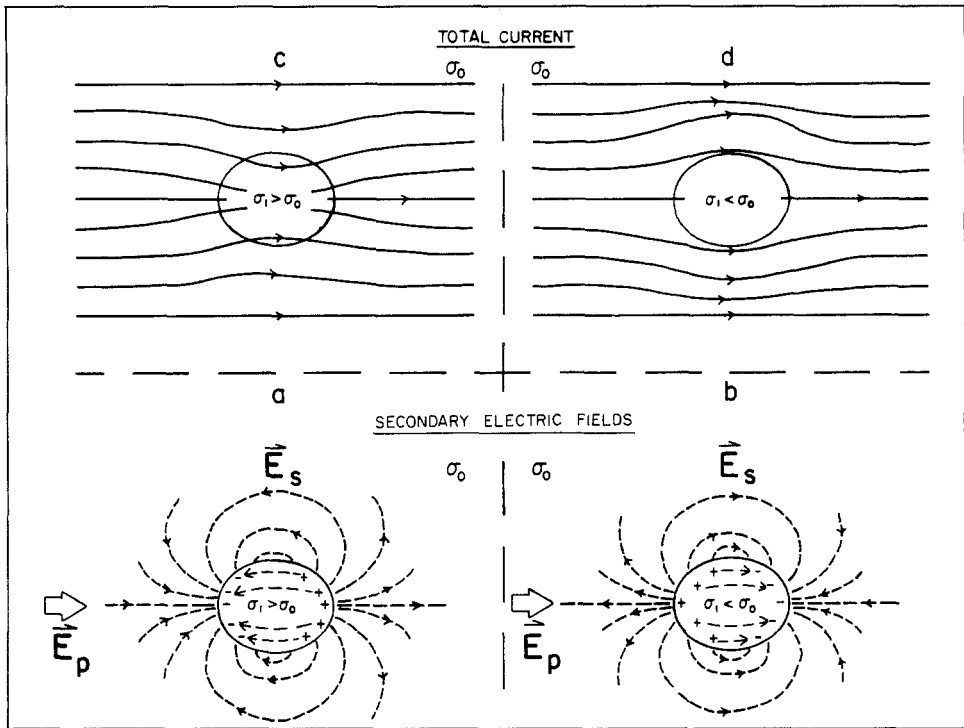


Fig. 1. Galvanic effect. Boundary charges form on surface of (a) conductive inclusion and (b) resistive inclusion producing secondary electric fields  $\vec{E}_s$  (dashed). Primary field  $\vec{E}_p$  and secondary fields  $\vec{E}_s$  add vectorially to produce total electric field  $\vec{E}$  resulting in (c) 'current channeling' and (d) 'current deflection' (modified after Wright, 1988).

sense of distortion in the resulting total electric fields. With a conductive surficial feature (Figure 1a), the total field is reduced directly over the body, it is enhanced off the ends of the body, and it is diminished along the sides. In the resistive case (Figure 1b), the total field is increased directly over the body, it is decreased off the ends, and an increase occurs along the sides of the body. Figures 1c and 1d present the resulting patterns of total current flow illustrating the classic cases of 'current channeling' and 'current deflection' around conductive and resistive inhomogeneities, respectively. Many authors describe the current paths, which are parallel to the total field lines, as shown in Figures 1c and 1d as being deflected by the charges. It seems more instructive to consider the total field as a vector sum of the primary and secondary fields. Then it is clear, e.g., that the total electric field is decreased over a surficial conductive body (Figure 1a) even though the current density is increased there (Figure 1c).

#### Static Shift

The previous phenomenon has been described in the Soviet literature as the S-effect since the process can be defined as a function of the integrated conductance (the

conductivity-thickness product) of the inhomogeneity. The S-effect has also been specifically defined as the upward or downward shift of magnetotelluric log-log apparent resistivity versus period sounding curves due to galvanic effects (e.g., Berdichevsky *et al.*, 1989).

The effects of boundary charge buildup are a reduction or an enhancement of the total electric fields at different locations. Therefore, MT sounding curves are shifted upward when measuring directly over surficial resistive bodies (Figure 1b) and they are depressed over conductive patches (Figure 1a). Along the side of a conductive body a sounding curve is shifted downward; it is shifted upward off the ends of the body, and so forth. These conclusions are based entirely on the distortions of the electric fields even though the apparent resistivity calculation is a function (the square) of the electric field divided by the orthogonal magnetic field. The magnetic field variations due to galvanic current deviations (Figures 1c and d) are calculated by volume integration of excess currents. Hence, the galvanic magnetic field distortion is small for small inhomogeneities; however, it could be significant in situations of large galvanic distortion (Groom and Bailey, 1989).

Figures 2 and 3 provide examples of magnetotelluric apparent resistivity soundings that are shifted vertically due to surficial inhomogeneities and topography, respectively. In the actual MT field data in Figure 2, the results are already displaced at the shortest periods. Here, the values approximating the transverse electric (TE) and transverse magnetic (TM) modes are shifted nearly parallel to each other up to 0.2 s period. Above 0.2 s, additional lateral effects superimpose to

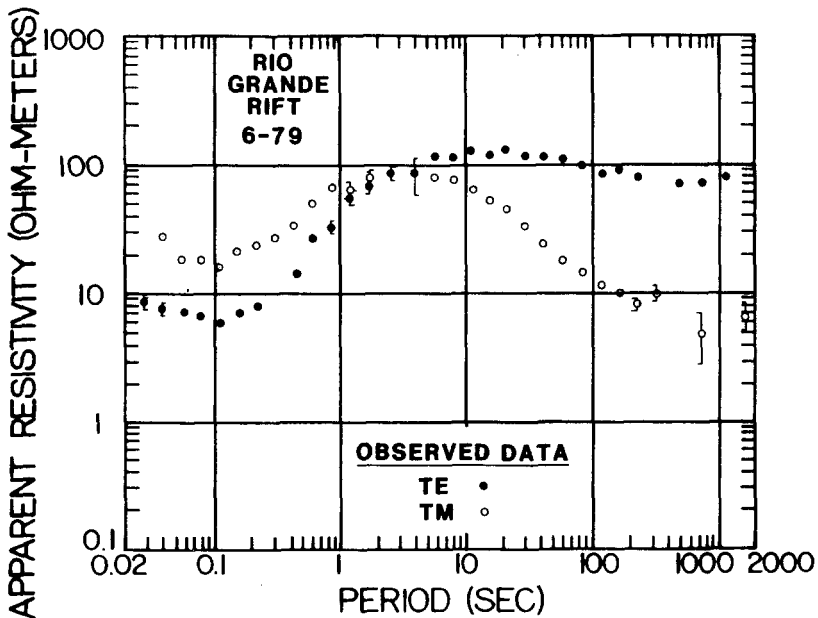


Fig. 2. Static shifts. Observed TE and TM apparent resistivity sounding curves in Rio Grande rift, U.S.A. showing short and long period MT static shifts (after Jiracek *et al.*, 1989b).

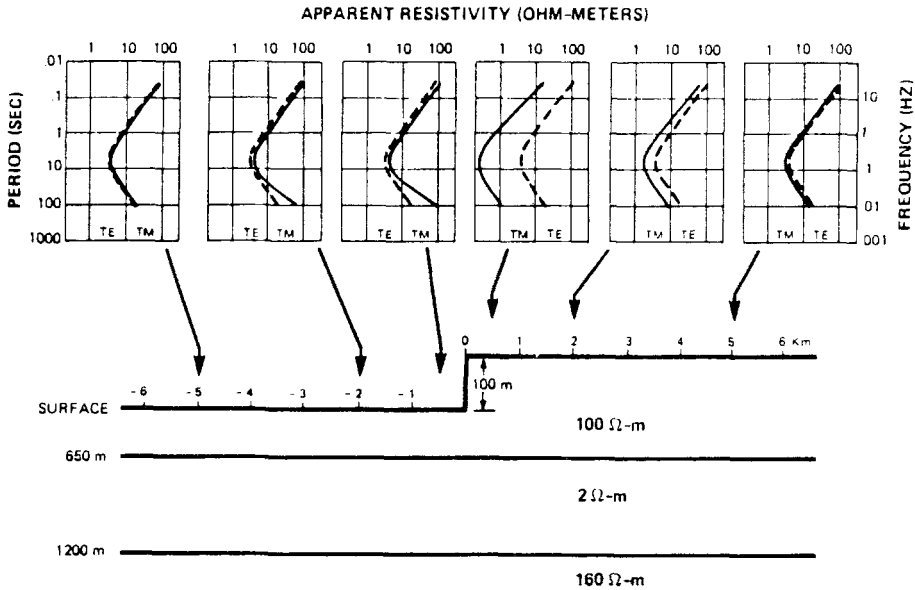


Fig. 3. Static shift due to topography. Theoretical TE and TM apparent resistivity sounding curves at various locations across a 2-D topographic step underlain by a layered earth (after Z-Axis Exploration, Inc. personal communication, 1982).

destroy the parallelism caused by the smaller, near-station features. The TE and TM curves in Figure 2 display a larger scale static shift above about 100 s period probably caused by other lateral boundaries some tens of kilometers away. In Figure 3 the theoretical shifting of apparent resistivity sounding curves is illustrated for different locations across a (2-D) topographic step.

The use of the term static shift for curve shifting probably stems from its association with the seismic statics correction which deals with surface weathering (inhomogeneities) and elevation (topography). The effect is asymptotically a constant (or static) shift, independent of frequency. This happens when the primary electric field that charges the inhomogeneity is uniform over the extent of the body. This is not true at high frequencies; e.g., if the skin depth in the host rock is less than the depth extent of the feature, the body is charged more near the top than at the bottom. As the frequency decreases, the increased skin depth results in a quasiuniform charging field that persists to dc. Thus, "one will never (get) rid of the S-effect no matter how low the frequency is chosen!" (Berdichevsky and Zhdanov, 1984). The major portion of this review describes various approaches to solve this dilemma approximately.

No distortion occurs in impedance phase curves over the period range where the galvanic effect is fully developed. This has been described as a remarkable fact. However, it can be understood simply since the secondary galvanic electric field due to an inhomogeneity (via Equation (2)) is in phase with the charging field (which at low frequencies is uniform and independent of frequency). Furthermore, the

secondary magnetic field is usually inconsequential, so the impedance phase is unaffected. The responses of other, neighboring bodies can destroy the parallelism of the apparent resistivity curves (Figure 2) and the equality of the phase results. Also, at higher frequencies, the skin depth dependence of the charging electric field invalidates the agreement of the distorted and undistorted impedance phase results.

### *Adjustment Distance*

The concept of adjustment distance (sometimes called the horizontal skin depth) was first described by Berdichevsky and Dmitriev (1976b) and Ranganayaki and Madden (1980). It has been reviewed previously by Jones (1983) and Menvielle (1988). Adjustment distance concerns vertical current distortion due to galvanic effects; in fact, Figure 1 can be used to appreciate this if the sketches are regarded as vertical cross-sections rather than plan views. The adjustment distance measures how easily vertical current flows into or out of a surface inhomogeneity (Park, 1985); however, it also addresses the question: "How far one should go away from any inhomogeneity in order to obtain information on the earth's deep structure?" (Fainberg and Singer, 1987). Ranganayaki and Madden (1980) showed that the answer to this question depends profoundly on the coupling between a conductive mantle and the surficial conductor through the resistive lower crust. Similar coupling through a resistive screen was studied earlier by Vanyan (1959, 1965). The adjustment distance decreases as the resistivity of the resistive layer decreases since vertical current flow is enhanced. The adjustment distance formulation contains exponential decay similar to the usual skin depth and is represented (Ranganayaki and Madden 1980) by

$$\lambda = (ST)^{1/2} = \left( \sum_{i=1}^n \sigma_i h_i \sum_{j=1}^m \rho_j h_j \right)^{1/2}. \quad (5)$$

Here,  $S$  is the integrated conductance of  $n$  surficial layers with conductivity-thickness products  $\sigma_i h_i$  and  $T$  is the integrated resistance of the underlying resistive sequence; each layer has a resistivity  $\rho_j$  and thickness  $h_j$ . Equation (5) is based on the approximation of generalized thin sheet analysis and has been confirmed by more exact formulations (Dawson *et al.*, 1982; Fainberg and Singer, 1987). The calculation of the adjustment distance is useful to estimate the relative portion of the excess current in a conductive surficial inhomogeneity that is due to lateral versus vertical current gathering. If the horizontal dimensions of the body are smaller than  $\lambda$  then the majority of the excess current is concentrated laterally. If the adjustment distance is the lesser, then vertical current gathering is the dominant macroscopic effect. It is stressed, that in any case, the underlying cause of any excess current is formation of charges along the sides and bottoms of surface features where there is a component of the total electric field vector perpendicular to the boundary (Equations (2) and (3)). Charges do not form on the top of the surface inhomogeneities unless there is surface roughness or topography.

### Galvanic Topographic Effect

Figure 4 illustrates the galvanic effect for an idealized 2-D hill-valley sequence. The galvanic effect in 2-D occurs when the primary electric field is perpendicular to the trend (or strike) of the topography. This is the TM mode or H-polarization which is always associated with galvanic effects. Charges form on the surface of the undulations in accordance with Equation (3). Although the vector total field in free space is required in this formula, one can obtain the correct charge polarity by simply considering the vector primary field. With this approximation one predicts (Figure 4a) that there are no charges at the top of the hill and at the bottom of the valley where  $\vec{E}_p \cdot \nabla\sigma = 0$ ; maximum charge concentration is where the surface slope is greatest, hence  $\vec{E}_p \cdot \nabla\sigma$  is maximum. As in the case with surface inhomogeneities (Figure 1), the total field is obtained by a vector sum of the primary and secondary fields. This gives the familiar galvanic total electric field pattern and current flow beneath surface topography (Figure 4b), which is completely tangential at the surface. There is finite (but spatially variable) electric field normal to the undulating surface in free space in order to satisfy Equation (3). The continuity of normal current density is still preserved (equal to zero) since the conductivity of free space is zero. From the directions of the secondary fields sketched in Figure 4a and from

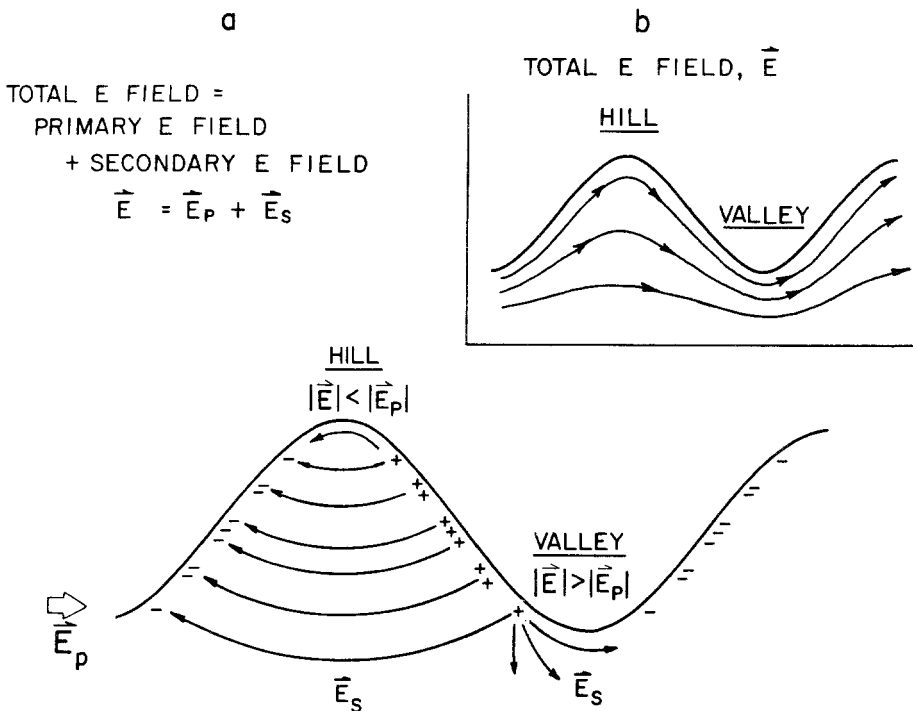


Fig. 4. Topographic galvanic effect. (a) Galvanic charge distribution (magnitude shown schematically) and resulting secondary fields  $\vec{E}_s$  for a hill-valley sequence. Primary field  $\vec{E}_p$  and secondary fields  $\vec{E}_s$  add vectorially to produce total electric field  $\vec{E}$  pattern shown in (b).

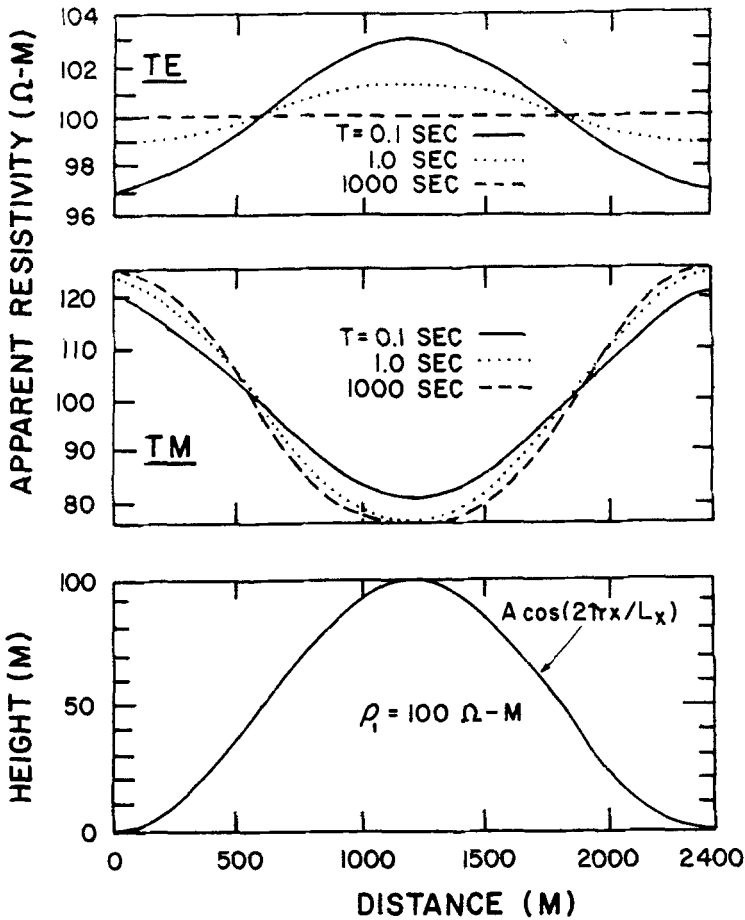


Fig. 5. Topographic TE and TM distortion. Theoretical TE and TM apparent resistivity increase and decrease, respectively, over cosinusoidal topography at different periods (after Reddig and Jiracek, 1984).

the macroscopic view of current distortion (Figure 4b) it is clear that electric fields are reduced on topographic hills and are increased in valleys due to the galvanic effect. Hence, the apparent resistivity values due to the galvanic effect are highest in valley troughs and lowest on topographic peaks (TM in Figure 3 and 5). Ironically, these are the locations of minimal charge accumulation (Figure 4a). A major difference between the galvanic effects of surface topography and surface inhomogeneities is precisely that the former need not be inhomogeneous for distortion to occur (e.g., Figures 3 and 5).

#### INDUCTIVE EFFECTS

The time derivative of the magnetic flux in Faraday's law results in the inductive response being an explicit function of frequency. The response function is, additionally, a function of the electrical properties and geometry. The overall dependency

for bodies of simple shape in free space is expressed by a dimensionless quantity called the induction number. For example, with the quasistatic approximation, for a spherical body it is equal to (Ward, 1967)

$$\theta = (\omega\mu_0\sigma)^{1/2}R. \quad (6)$$

Here,  $\omega$  is the angular frequency  $2\pi f$ ,  $\mu_0$  is the magnetic permeability, and  $R$  is the radius of the sphere. In induction, the time varying primary magnetic field produces a voltage which induces vortex currents to flow in a closed body. The spatial relationship and the resulting secondary magnetic field  $\vec{H}_s$  are sketched in Figure 6. The galvanic charges formed on the edges of the thin vertical sheet are also included in Figure 6.

The inductive effect is unlike the galvanic effect where the secondary electric field is in phase with the causative primary electric field (Equation (3)). In fact, the phase of the secondary magnetic field varies between 0 and  $\pi/2$  relative to the primary magnetic field. This well-known (e.g., Ward, 1967; Lajoie and West, 1976; Morrison *et al.*, 1976) inductive response can be expressed as a function of the induction number. In the limiting case of small induction number and low response, the phase is  $\pi/2$  (the resistive limit). At high induction number there is a large, in-phase response which is termed the inductive limit. The magnitude of the inductive effect increases toward saturation as frequency increases; this is just the opposite of the galvanic effect which increases toward saturation with decreasing frequency.

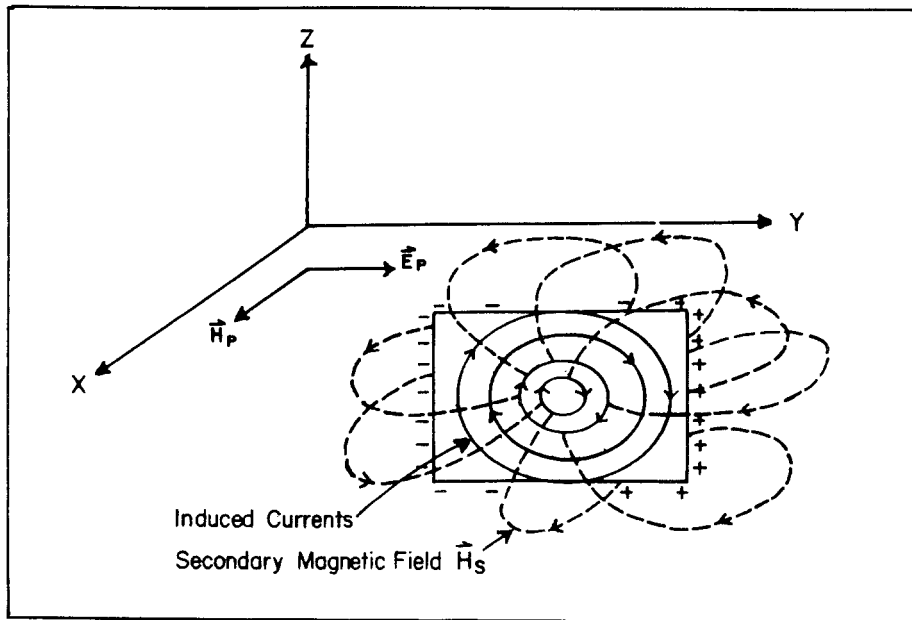


Fig. 6. Inductive effect. Induced vortex currents in vertical sheet conductor produce dipolar secondary magnetic field  $H_s$  pattern. Charges shown are due to the galvanic effect (after Wright, 1988).

Another major difference in the two effects is the underlying lead role of the electric field in the galvanic case in contrast to that of the magnetic field in induction.

The foregoing discussion of the inductive effect neglects the conductivity of the material surrounding an isolated body. For nonzero host conductivity a combination of inductive and galvanic effects results in the 'leaking out' of the current vortex (Figure 6) into the host. The proportions of vortex and gathered current flow and the phase considerations are strongly dependent on the conductivity of the host (Lajoie and West, 1976).

The spatial orientation of the secondary magnetic field lines in conjunction with the primary magnetic field (Figure 6) can be used to estimate the total magnetic field effect just as the electric fields were used in the galvanic case (Figures 1 and 4). For example, directly over the conductive body in Figure 6, the total magnetic field is increased since  $H_s$  is in the same direction as  $H_p$ . It is also clear that a vertical magnetic field component is produced away from the body since the secondary magnetic field has a dipolar pattern. One must also evaluate the electric field distortion in the inductive case, e.g., if electric field measurements were made in the  $y$  direction along the outcropping thin sheet in Figure 6. However, surficial EM inductive effects are not nearly as troublesome in deep soundings as are galvanic distortions since they disappear as frequency decreases. Inductive effects are diminished for reduced induction number (Equation (6)) so either low frequency or small size results in the dissipation of inductive effects.

The TE or inductive response of a 2-D surface inclusion in a layered earth has been presented by Berdichevsky and Zhdanov (1984) based on the earlier work of Dmitriev *et al.* (1973). A significant inductive distortion occurs when sounding over a resistive block adjacent to a surficial conductive zone. This is the problem of a 'false conductive layer' (Berdichevsky and Dmitriev, 1976b) when using TE data and 1-D analysis. Figure 7 illustrates this effect for the simple model of a 2.4 km deep, 1 ohm-m conductive basin and an MT sounding located 2.5 km away. The ascending branch (S-interval) of the TE sounding curve has been depressed mainly due to decreased total  $E$  field resulting from excess current flow in the conductor. A 1-D analysis of the TE curve in Figure 7 (Jiracek *et al.*, 1983) falsely predicts a conductive zone at 3 km depth. The inductive distortion illustrated in Figure 7, particularly its attendant vertical and horizontal magnetic field distortion, is the basis of the so called 'coast effect' when EM soundings are made adjacent to an ocean (Parkinson and Jones, 1979).

There have been suggestions that inductive effects can be calculated by application of the Biot-Savart law particularly in 2-D situations. However, Jones (1986) has shown that the ensuing approximation of line current sources in free space is invalid for a finite conducting host except in very close proximity to a current source.

Adam *et al.* (1986) have used the Biot-Savart law to estimate the magnitude of TE topographic effects compared to deeper anomalies. A more rigorous evaluation of the TE inductive response of topography has been made by applying the

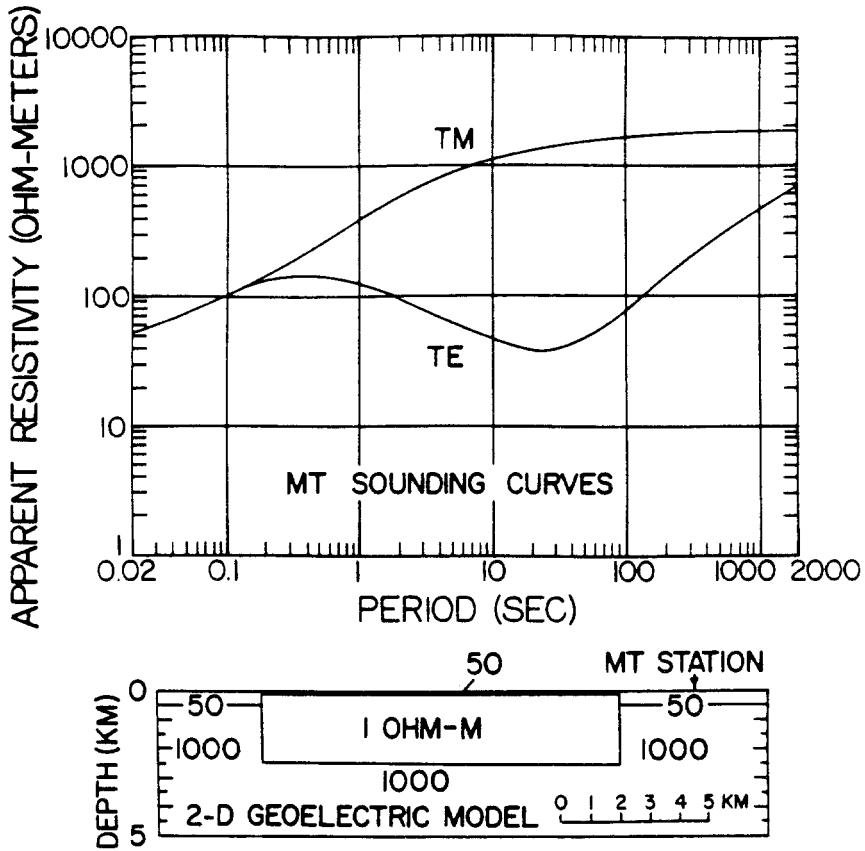


Fig. 7. 'False conducting layer' in TE curve. Shallow 2-D conductive basin-like geoelectrical model and synthetic TE and TM sounding curves at nearby MT station (after Jiracek *et al.*, 1983).

Rayleigh-FFT method (Reddig and Jiracek, 1984; Jiracek *et al.*, 1989b). The final result is that the apparent resistivity (and impedance) increases on hills and decreases in valleys (Figure 5). This is the exact opposite distortion to the galvanic effect but the magnitude is much less than the galvanic effect and the inductive effect disappears at long periods (Figure 5). It is interesting that, e.g., over a 2-D hill, both the total TE electric and magnetic fields are significantly increased but by nearly the same relative amounts. Therefore, their ratio (which yields the impedance and apparent resistivity) is little affected.

FINITE LENGTH ELECTRIC FIELD LINES

The actual electric field measurement is made with two earth contacts connected to a voltage measuring device by finite lengths of wire. The measured voltage  $V$  is, therefore

$$V = \int_{l_1}^{l_2} \mathbf{E} \cdot d\mathbf{l} \tag{7}$$

where  $d\mathbf{l}$  is an elemental length along the ground between points  $l_1$  and  $l_2$ . Gomez-Trevino (1987) has discussed the dependency of the voltage measurement (Faraday's law) when the connecting cable is not straight. Poll *et al.* (1989) have suggested that voltage differences divided by the  $l_2-l_1$  separation rather than electric fields calculated by numerical codes should be used in 2-D TM computer modeling. This recognizes the distortions inherent in electrical field measurements if Earth contact is in two different media.

Equation (7) represents an average value of the electrical field over the cable contour and as such is a low pass filter. The process can be expressed as a spatial low pass filter with a 'box car' impulse response function (Torres-Verdin and Bostick, 1989). This aspect of the electric field measurement will be discussed further in regard to the EMAP method. For now, one should realize that the spatial variations of electric fields due to both galvanic and inductive effects are smoothed by using finite length dipoles in accordance with Equation (7). The longer the dipole length, the lower the spatial passband of the effective filter. Consequently, long electric field lines can considerably reduce any small scale electric field distortions. Sternberg *et al.* (1988) and Pellerin (1988) contain excellent examples of this result. For example, they show that if a dipole length is four times the width of a centered conductive body, the static shift is less than 1/10 of a decade in apparent resistivity.

### Distortion Correction Techniques

Techniques proposed to correct for the unwanted galvanic and inductive distortions due to near-surface inhomogeneities and topography can be loosely classified under six categories. In an approximate order of complexity these are: use of invariant response parameters, curve shifting, statistical averaging, spatial filtering, use of distortion tensors, and computer modeling.

#### INVARIANT PARAMETERS

Two rotationally invariant impedance functions have been used for some time (Berdichevsky and Dmitriev, 1976b) to calculate an 'effective impedance'. The 'Berdichevsky average'  $Z_B$  is the arithmetic mean of the off-diagonal components of the impedance tensor,

$$Z_B = (Z_{xy} - Z_{yx})/2. \quad (8)$$

The determinant of the tensor yields another effective impedance

$$Z_D = (Z_{xx}Z_{yy} - Z_{xy}Z_{yx})^{1/2}. \quad (9)$$

In these relations,  $Z_{ij}$  are the complex elements of the usual two by two impedance tensor. Advantages of using this approach are that no mode identifications (TE or TM) are required, static shifts or other corrections are not made, and the dimensionality of the data is not considered (Reddig *et al.*, 1989). The idea is that the

effective impedances can be interpreted as 1-D for initial point by point modeling. The physical basis for using an effective impedance is that apparent resistivity curves that are oriented in two different directions develop opposite static shifts when calculated near isometric inhomogeneities (Berdichevsky *et al.*, 1989). Thus, one would consider an additional orthogonal orientation of the incident electric field in Figure 1. Livelybrooks (1986) and Reddig *et al.* (1989) report good agreement between 1-D modeling of effective impedances and some true multi-dimensional models. However, Reddig *et al.* (1989) additionally filter the effective results.

There are many examples of the shortcomings of using effective impedances. Figure 8 from Pellerin (1988) provides such an example. Figure 8a contains the overall model of a large 3-D  $10\ \Omega\cdot\text{m}$  body embedded in a 1-D, layered earth. A small 5 m thick,  $5\ \Omega\cdot\text{m}$  surficial inhomogeneity is located as shown. The distorted apparent resistivity curves  $\rho_{xy}$  and  $\rho_{yx}$  are presented in Figure 9 as calculated by 100 m long crossed dipoles located over the small body (Figure 8b). The true,

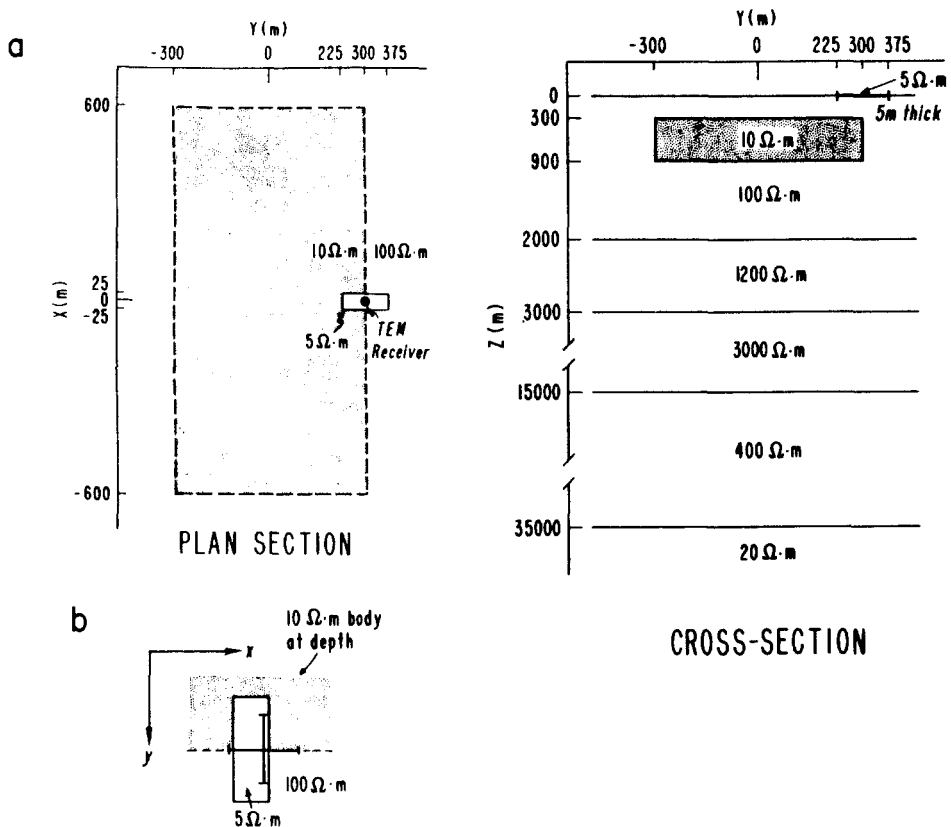


Fig. 8. (a) Geometry of 3-D  $5\ \Omega\cdot\text{m}$ , 5 m thick conductive surficial inhomogeneity and a large, deeper 3-D  $10\ \Omega\cdot\text{m}$  body in a layered earth. Locations of (a) central-loop TEM receiver and (b) 100 m crossed MT electrode array are shown (after Pellerin, 1988).

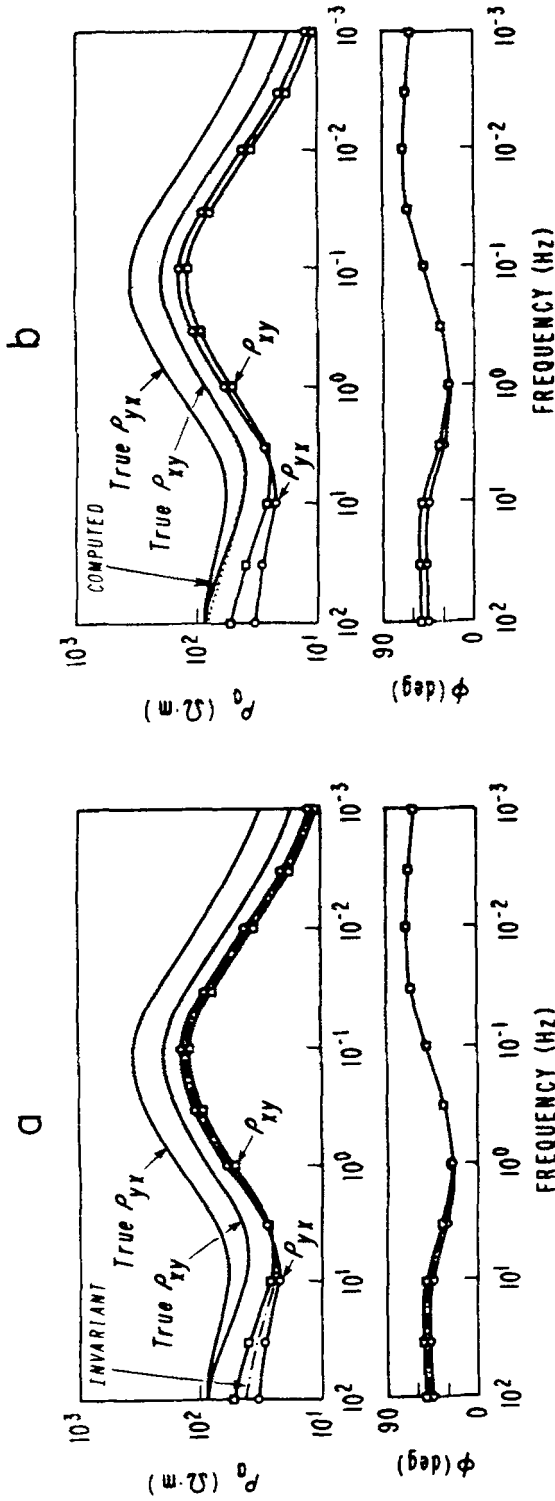


Fig. 9. (a) Unsuccessful removal of surficial distortion using invariant sounding curve. Synthetic  $\rho_{xy}$ ,  $\rho_{yx}$ , and invariant curves calculated for 3-D model in Figure 8. True curves are calculated without surficial body. (b) Successful computation of correction curve for curve shifting. Synthetic  $\rho_{xy}$ ,  $\rho_{yx}$ , and true curves as in (a). Computed correction curve to which distorted  $\rho_{xy}$  and  $\rho_{yx}$  would be shifted is from synthetic TEM sounding (after Pellerin, 1988).

undistorted apparent resistivity curves are presented in Figure 9a along with the results calculated by both invariant impedances. In this case the invariant curve is still depressed, it does not remove the static shift, and the 1-D interpretation of it would provide an incorrect interpretation.

Groom and Bailey (1989) have shown that the  $Z_D$  calculation for surficial 3-D galvanic distortion in an otherwise regional 1-D or 2-D structure is simply static shifted compared to the true regional result. However,  $Z_B$  is an unknown combination of the regional principal impedances.

### CURVE SHIFTING

In a certain sense, most of the distortion removal techniques can be described as curve shifting procedures. The concept is simple enough. The distorted curves (e.g., in Figures 2, 3, and 9a) are shifted into coincidence with the true, correct, undistorted curve (Figure 9b). If the distortions are truly static then vertical shifts would suffice. Each curve is shifted by different amounts in the general 3-D case (e.g., Figure 9b). When surficial inhomogeneities or topography are quasi 2-D (i.e., long compared to the skin depths involved) then only the TM curves need to be shifted. Since the distorting features tend to be small, the problem is usually 3-D and shifting only the curve identified as approximately TM is incorrect.

Jones (1988) has shown the value of shifting the TE and TM soundings into agreement with the modal resistivity value characteristic of a known layer within a sedimentary basin. This is possible if many observations are available and the layer resistivity can be treated in a parametric form along the profile. This limits Jones' approach but the method does not suffer from the requirement of auxiliary soundings as proposed by many authors.

Andrieux and Wightman (1984) showed that static shifts can be made by measuring the resistivities in the upper section by electromagnetic methods, specifically by transient or time domain EM soundings (TEM). Sternberg *et al.* (1985, 1988) use a similar procedure, citing the fact that a measurement involving the magnetic field is less affected by small-scale inhomogeneities. This is true of the galvanic effect as discussed earlier. Sternberg *et al.* (1988) also jointly invert the TEM and TM data with a 1-D computer code that includes a vertical MT static shift parameter but does not address any multi-dimensional modeling. Pellerin (1988) has quantified the value of TEM soundings to correctly shift MT sounding curves based on 1-D inversion of central loop TEM soundings. Figure 9b contains the computed 1-D MT response curve at high frequencies resulting from the estimated geoelectric section obtained from a synthetic TEM sounding centered over the 3-D surface distorting feature in Figure 8. The computed curve approximates the true  $\rho_{xy}$  data very closely. This is because, for the elongated 10  $\Omega$ -m body at 300 m depth (Figure 8), the  $\rho_{xy}$  data are a good approximation of the ideal 2-D TE response. Shifting both of the distorted  $\rho_{xy}$  and  $\rho_{yx}$  curves in Figure 9b to agreement with the computed value at 100 Hz would very nearly recover the true  $\rho_{xy}$  and  $\rho_{yx}$  curves. However, as discussed by Pellerin (1988), within the period of

MT and TEM overlap, the distorted and computed curves are not parallel. Therefore, the procedure based on 1-D TEM inversion cannot be completely valid. Parallel  $\rho_a$  curves and the equality of impedance phases are required over a sufficient frequency range. This is determined by the overlap between the minimum MT skin depth and maximum depth of penetration of TEM soundings. Spies and Frischknecht (1989) have discussed the superior depth-to-lateral investigation ratio of the central loop technique. Using TEM soundings to correct for static shifts does require another extra survey. However, the TEM soundings can be made after the MT survey and only at stations exhibiting static effects.

Wolfegram and Scharberth (1986) describe a technique called ECRE (Electrical Conductivity Reference Exploration) where they apply geomagnetic depth sounding (GDS) principles to correct for local distortions. This technique based on natural magnetic field measurements has the disadvantage of greater lateral sensitivity compared to controlled source methods. Since the GDS primary magnetic field is horizontal compared to vertical in the TEM method, it would be sensitive to vertical sheets, e.g., fissures, fractures, dikes but it is not as revealing of horizontal inhomogeneities. The vertical magnetic field required in the ECRE method is now routinely measured but high audio recordings would be necessary to implement the procedure.

There are several case histories of using auxiliary EM soundings to correct distorted MT curves beginning with Andrieux and Wightman (1984). Sternberg *et al.* (1988) have tested the use of a Sirotem TEM system, a Phoenix IPV3 frequency

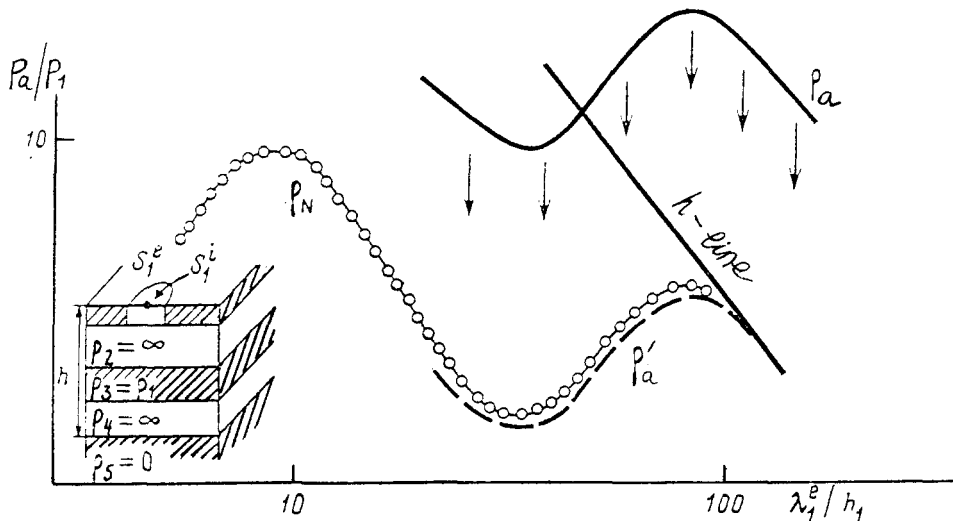


Fig. 10. Correction of distorted MT  $\rho_a$  curve by shifting to long period normal branch. Synthetic  $\rho_a$  curve obtained over a resistive inclusion  $S_1^i$  in an otherwise layered earth. Normal curve  $\rho_N$  is calculated without inclusion. Corrected curve  $\rho'_a$  obtained by shifting  $\rho_a$  curve to coincidence with long period descending branch ( $h$ -line) (after Mikhlin, 1984; presented in Berdichevsky *et al.*, 1989).

domain unit, and a Geonics EM37 TEM unit in making the corrections. Examples given by Sternberg *et al.* (1988) from a complex, topographically rough area in central Oregon, USA have static shifts averaging 3/4 to 4/10's of a decade. An example of the ECRE method is given by Jensen and Seara (1988) over a 2-D salt structure.

Another, quite different, curve shifting analysis has been applied by MT researchers in the Soviet Union. Instead of shifting sounding curves into coincidence with an appropriate short period segment, the procedure is applied to an asymptotic long period branch (Rokityansky, 1982; Berdichevsky *et al.*, 1989). The central idea is that there is sufficient invariability of the geoelectric section below 250–300 km depth that all soundings should approach the so-called standard or global apparent resistivity curve. This curve is obtained from global magnetovariation soundings using the worldwide network of geomagnetic observatories and selected long period MT soundings in stable regions. Figure 10 provides a theoretical example of such a means of shifting an MT sounding curve that is distorted by a near-surface S-shell as reported by Mikhlin (1984) and described by Berdichevsky *et al.* (1989).

#### STATISTICAL AVERAGING

Surficial inhomogeneities and topography can be looked upon as geologic noise which contaminates the desired signal. Hence, application of filter theory to remove the unwanted effects is natural. Statistical averaging is the simplest application of this approach.

There are many examples illustrating the random nature of the distribution of surficial anomalies. Figure 11 contains a portion of the over 300 effective MT soundings in the Baikal region of the USSR (Berdichevsky *et al.*, 1980) and a group of TM soundings from the Canadian Lithoprobe experiment on Vancouver Island (Kurtz *et al.*, 1986). The Baikal soundings are grouped according to their areal proximity and conformal, but shifted, shapes. The shifted soundings in the Canadian example are distorted primarily by galvanic effects, therefore, the impedance phase curves are nearly coincident (e.g., Figure 11a).

Simple geometrical averaging of the apparent resistivity values and arithmetic averaging of the phase data yielded a single smoothed sounding for each of the groups in Figure 11b. Subsequent 1-D modeling of the averaged curves then provided a regional interpretation. There is obviously a degree of subjectivity in how large an area is averaged and, under any circumstances, one loses some details that may have local and regional significance. Additionally, a considerable amount of data are required for effective statistical averaging. In fact, a large data set may be necessary in all areas of high complexity.

#### SPATIAL FILTERING

Averaging is a spatial filtering process but here it is considered separate from more extensive filtering schemes.

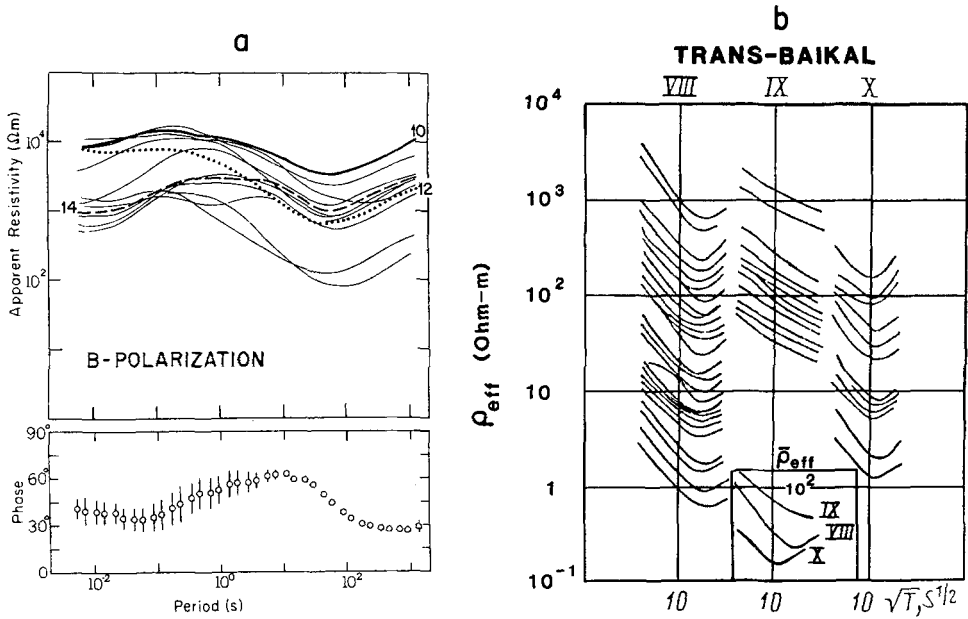


Fig. 11. Conformal but shifted apparent resistivity sounding curves. (a) TM apparent resistivity curves obtained in Canadian Lithoprobe project and average impedance phase values with one standard deviation indicated (after Kurtz *et al.*, 1986). (b) Three groups of effective  $\rho_a$  curves and their averages from zones VIII–X in the Trans-Baikal, U.S.S.R. (after Berdichevsky *et al.*, 1980).

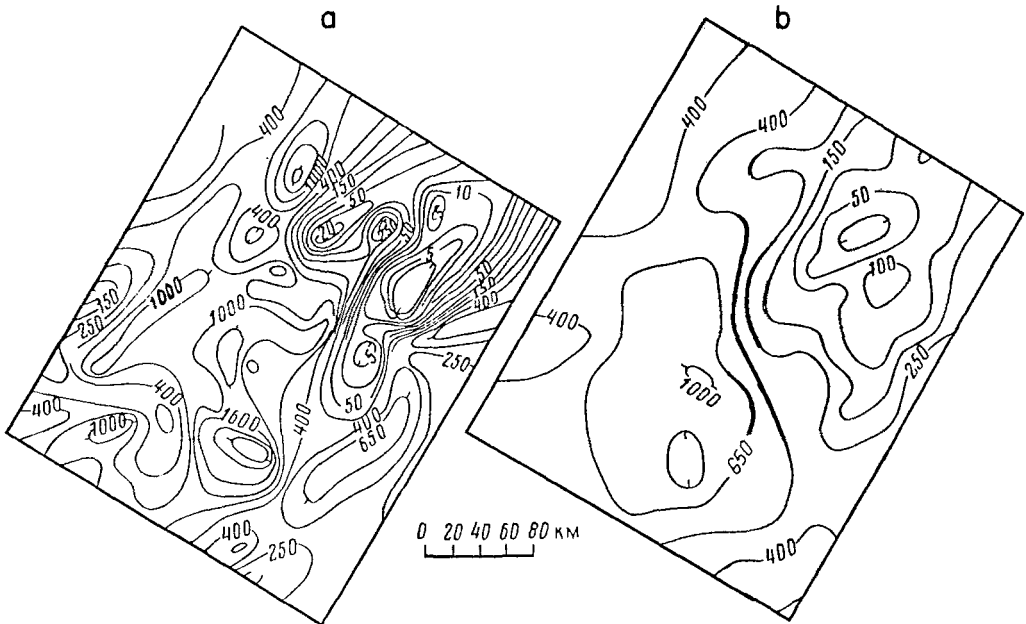


Fig. 12. Two-dimensional spatial filtering. (a) Map of observed apparent resistivity  $\rho_a$  data at 255 s period in Southern Yakutiya, U.S.S.R. (b) Map of  $\rho_a$  data after low pass filtering. Values in  $\Omega\text{-m}$  (after Berdichevsky *et al.*, 1989).

In exactly the same way that 2-D spatial wavenumber filtering has been applied to gravity and magnetic potential field anomalies, magnetotelluric data have been filtered (Berdichevsky *et al.*, 1989). Figure 12a presents a contour map of the observed TE apparent resistivity data and Figure 12b contains the data after low pass filtering. A 2-D filter designed with regard to the standard curve was applied to the raw data using a circular template. This, of course, is a convolution operation which could be studied in terms of its spatial frequency characteristics after Fourier transform (Fuller, 1967).

A new MT spatial filtering method has recently emerged in the United States that is motivated by the first-order Born approximation. The principles of the EMAP (ElectroMagnetic Array Profiling) method were developed by F. X. Bostick, Jr. after he linearized the relationship between the earth conductivity and surface electric field measurements (Bostick, 1986). The electric field when the source electric field excitation is in the  $x$  direction is given in the spatial frequency domain by

$$E(\omega, k_x, k_y) = G(\omega, k_x, k_y, z) \Delta\sigma(k_x, k_y, z). \quad (10)$$

Here,  $\omega$  is the usual angular frequency,  $k_x$  and  $k_y$  are the wavenumbers in the  $x$  and  $y$  directions, and  $z$  is the vertical direction. The function  $G$  is the response function obtained by spatial Fourier transform of the Green's function relating  $E(x, y, z)$  to  $\Delta\sigma(x, y, z)$ . The latter quantity is the perturbation of the conductivity about its average value  $\sigma_0$ . The 2-D Fourier transform of the conductivity perturbation appears in Equation (10). Although the requirements of the Born approximation leading to equation 10 are not satisfied in the actual earth (e.g.,  $\Delta\sigma \ll \sigma_0$  usually does not hold), the study of its ramifications are highly revealing. As shown by Torres-Verdin (1985) and Bostick (1986), in the 2-D earth situation (with  $y$  parallel to strike) the  $G$  response function for the TM mode is

$$G(\omega, k_x, 0, z) = (\omega\mu_0\sigma_0/k_z) e^{-i(k_z+k)z} + (k_x^2/ik_z) e^{-i(k_z+k)z}. \quad (11)$$

In the 3-D earth case

$$G(\omega, k_x, k_y, z) = (\omega\mu_0\sigma_0/k_z)(r_2) e^{-i(k_z+k)z} + (k_x^2/ik_z) e^{-i(k_z+k)z}. \quad (12)$$

In the above

$$k_z = (k^2 - k_x^2 - k_y^2)^{1/2} \quad (13)$$

$$k^2 = -i\omega\mu_0\sigma_0, \quad (14)$$

and  $1/2 \leq r_2 \leq 1$ .

The permeability of free space is  $\mu_0$ . As discussed by Bostick (1986), the first terms in the 2-D TM and 3-D response functions (Equations (11) and (12)) are similar to the 1-D and 2-D TE  $G$  representations not presented here. The 1-D and 2-D TE terms decrease with decreasing  $\omega$  and as such behave as inductive effects. The second terms in Equations (11) and (12), on the other hand, are independent

of frequency as  $\omega \rightarrow 0$  as is the galvanic effect. As  $\omega$  and  $z$  approach zero these terms act as high-pass spatial filters of the shallow conductivity variations. The inductive terms, on the other hand, are low-pass filters to the wavenumber components of the surficial conductivity perturbations.

EMAP is based on the concept of attenuating the galvanic components of the electric fields by spatially low-pass filtering the high-pass characteristics of the Green's functions in 2-D TM and 3-D MT responses. To accomplish this without spatial aliasing, the EMAP method requires a continuous dipole array of electric field sensors (Figure 13). It is recognized (see section on Finite Length Electric Field Lines) that dipolar sensing itself, imposes a spatial low pass on the electric field measurements. In addition, the outputs of adjacent dipoles are combined with appropriate weights to form additional low-pass filtering. The effective response of this latter step depends on the weights, the dipole length, and the number of sensors used. The total length of the filter (its window) is calculated using an apparent depth of penetration (Bostick, 1977). For example, when the apparent depth of penetration is large (say several kilometers), many short dipole outputs are combined to produce a single filtered output. Electric field measurements need not be made simultaneously but are instead referenced to single or multiple horizontal magnetic field sensors. Bostick (1986) argues that since the galvanic distortions due to the electric fields are removed by EMAP filtering, the resulting data can be inverted directly for deep structure. Impressive theoretical examples have been obtained using simple 1-D inversions.

Figures 14 and 15 present two theoretical examples of the application of the EMAP method from Torres-Verdin and Bostick (1989). Only one frequency

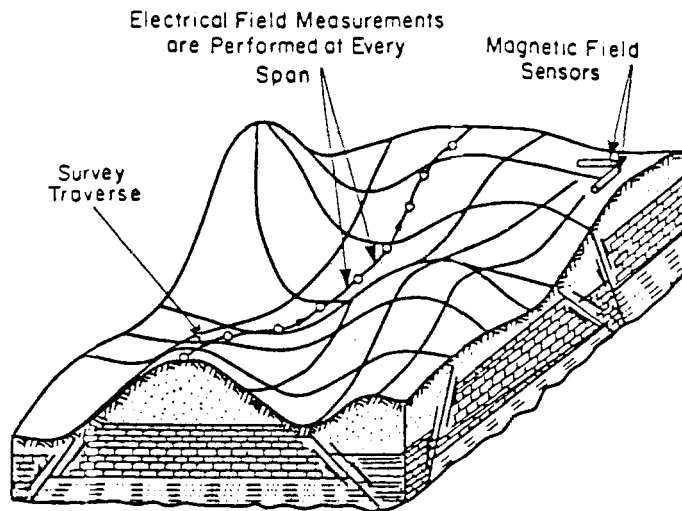


Fig. 13. EMAP data collection procedure. Continuous electric field data are acquired along survey lines and are referenced to nearby magnetic measurements (after Torres-Verdin, 1985).

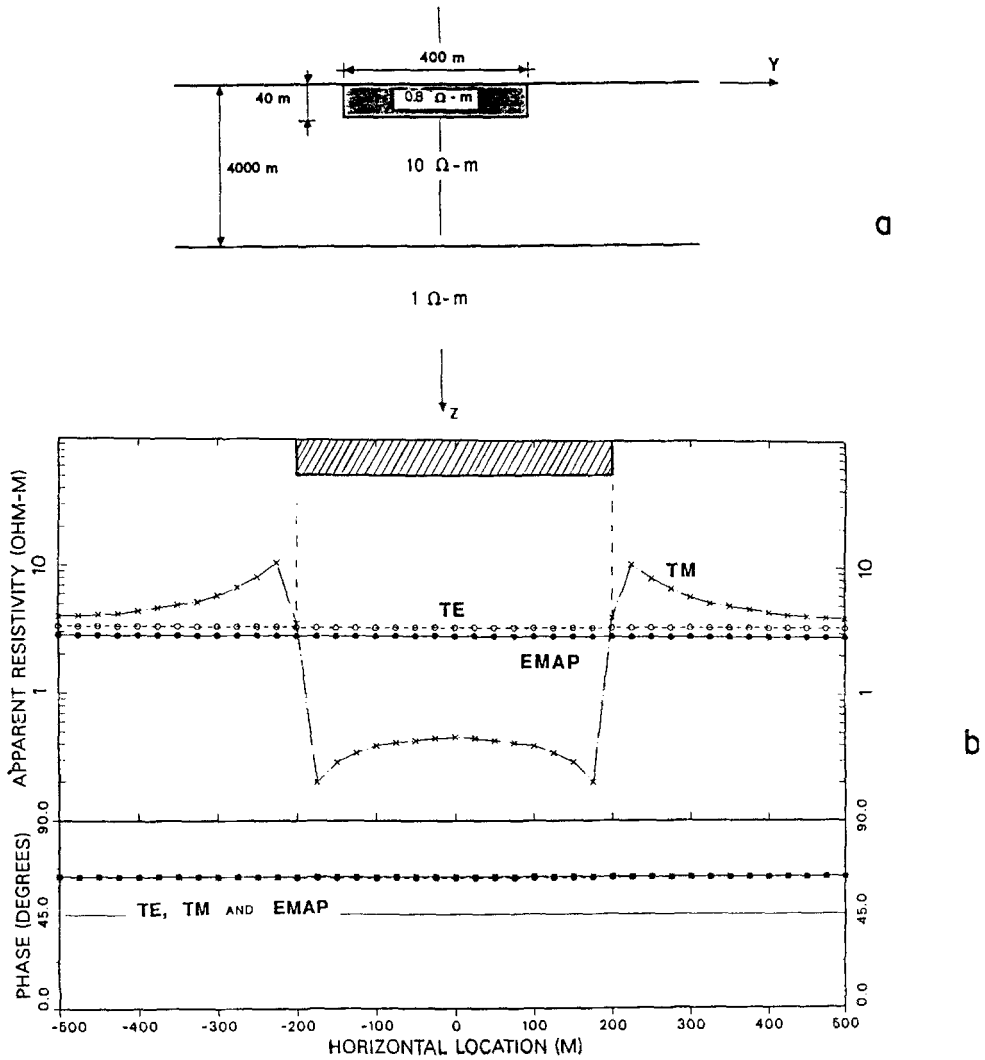


Fig. 14. Theoretical EMAP example with surficial inhomogeneity. (a) Geometry of 0.8  $\Omega$ -m, 40 m thick conductive surficial inhomogeneity in layered earth. (b) TE, TM, and EMAP apparent resistivity and impedance phase values across model in (a) at period of 100 s (after Torres-Verdin and Bostick, 1989).

(0.01 Hz) is considered in each case. The first case illustrates the removal of a 40 m deep surface feature in the 2-D TM mode closely yielding the appropriate TE result. The phase results are unaffected as is expected for the galvanic effect. In the second example (Figure 15), the synthetic TM response over 2-D topography has been filtered in a similar fashion. Figure 16 presents the final results after EMAP data collection and processing of MT data from mountainous terrain in Colorado, U.S.A. (Word *et al.*, 1986). The EMAP measurements were made using 53 electric field dipoles of 800 ft (244 m) length and one central magnetic reference station.

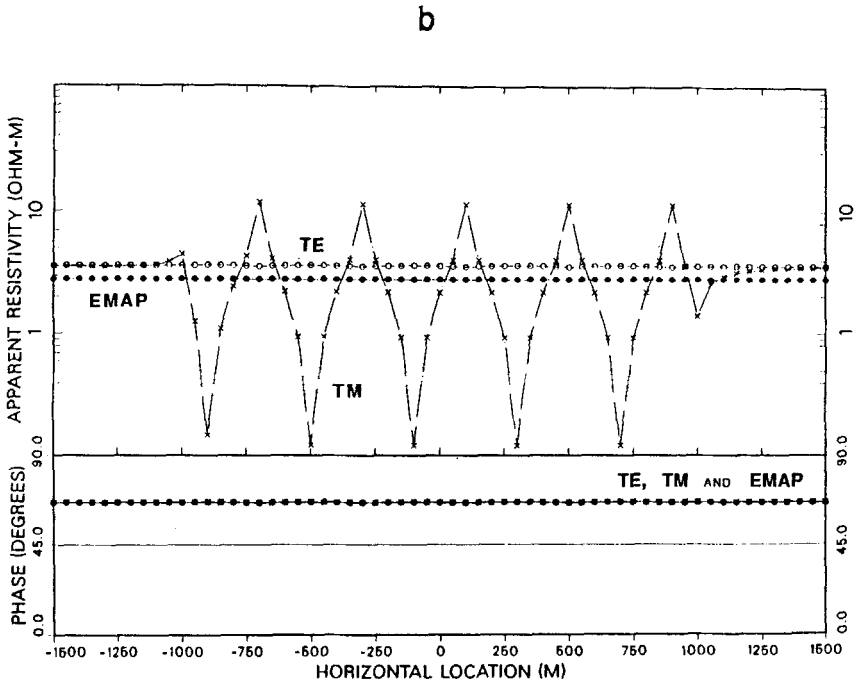
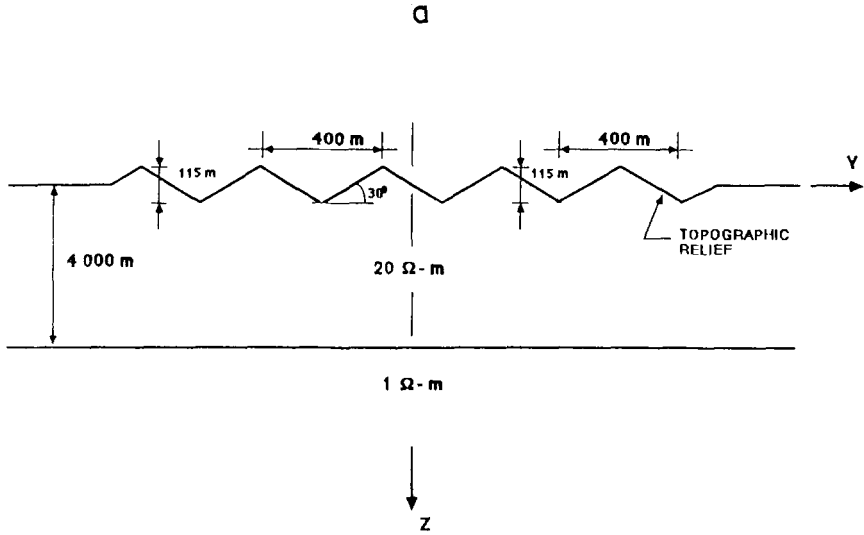


Fig. 15. Theoretical EMAP example with topography. (a) Geometry of 'saw-tooth' topography over layered Earth. (b) TE, TM, and EMAP apparent resistivity and impedance phase values across model in (a) at period of 100 s (after Torres-Verdin and Bostick, 1989).

The geoelectric section produced from EMAP is compared in Figure 16b to the downhole electric log results at two nearby oil wells. The comparison is quite favorable and, for example, clearly reveals  $\sim 7000$  ft (2133 m) thick resistive Precambrian rocks overthrusting conductive Mesozoic strata in the Champlin Bear Springs well.

The EMAP method is proposed as a profiling technique run roughly perpendicular to strike with end to end dipoles. Occasional measurements of the vertical magnetic field along the line are required to sense inductive effects off-line to guard against effects such as those of the 'false conductor' in Figure 7. Continuous profiling is very laborious and it may be logistically untenable in some circumstances. Also, there may be good reason in complex 3-D environments to do EMAP surveying in an areal rather than a profile mode. This certainly impacts the practicality of continuous electric field measurements. Then too, the spatial processing of the data imposes certain filter response functions with attentive compromising of the vertical and horizontal resolution. However, EMAP may become a routine MT tool for hydrocarbon prospecting in the U.S.A. where spatial aliasing resulting from point to point sampling in traditional MT collection cannot be tolerated. Reddig *et al.* (1989) effectively apply EMAP-like spatial low pass filtering to standard, closely spaced MT stations along a profile in their MT Frequency Domain Imaging (MTFDI) method.

#### DISTORTION TENSORS

Following the lead of Schmucker (1970) and Larsen (1977) who formulated expressions relating the distorted and undistorted fields in terms of a distortion tensor, Mozley (1982) applied the concept to remove the effects of topography from MT data. Distortion tensor stripping of topographic effects is in the realm of possibility since topography is known. However, since the terrain resistivity may vary and near-surface inhomogeneities have unknown geometries, stripping of these features is risky. This would be akin to making a seismic statics correction with improper velocity or weathering information.

Jiracek *et al.* (1989b) have expressed the relationship between the components of the distorted electric field ( $E^D$ ) and the undistorted ( $E^U$ ) ones in the general form

$$\begin{bmatrix} E_x^D \\ E_y^D \\ E_z^D \end{bmatrix} = \begin{bmatrix} D_{xx}^E & D_{xy}^E & D_{xz}^E \\ D_{yx}^E & D_{yy}^E & D_{yz}^E \\ D_{zx}^E & D_{zy}^E & D_{zz}^E \end{bmatrix} \begin{bmatrix} E_x^U \\ E_y^U \\ E_z^U \end{bmatrix}. \quad (15)$$

The  $3 \times 3$  distortion tensor  $[D]$  is complex, frequency dependent in general; a similar relation to Equation (15) relates the magnetic fields. To estimate the distortion tensor elements from the distorted field values one must model the unwanted surficial effects (topography and other features) and assume an undistorted model, usually a flat, homogeneous half-space. Since this latter step assumes no *a priori* knowledge of the subsurface, it neglects any electromagnetic coupling between the distorting features and the subsurface targets.

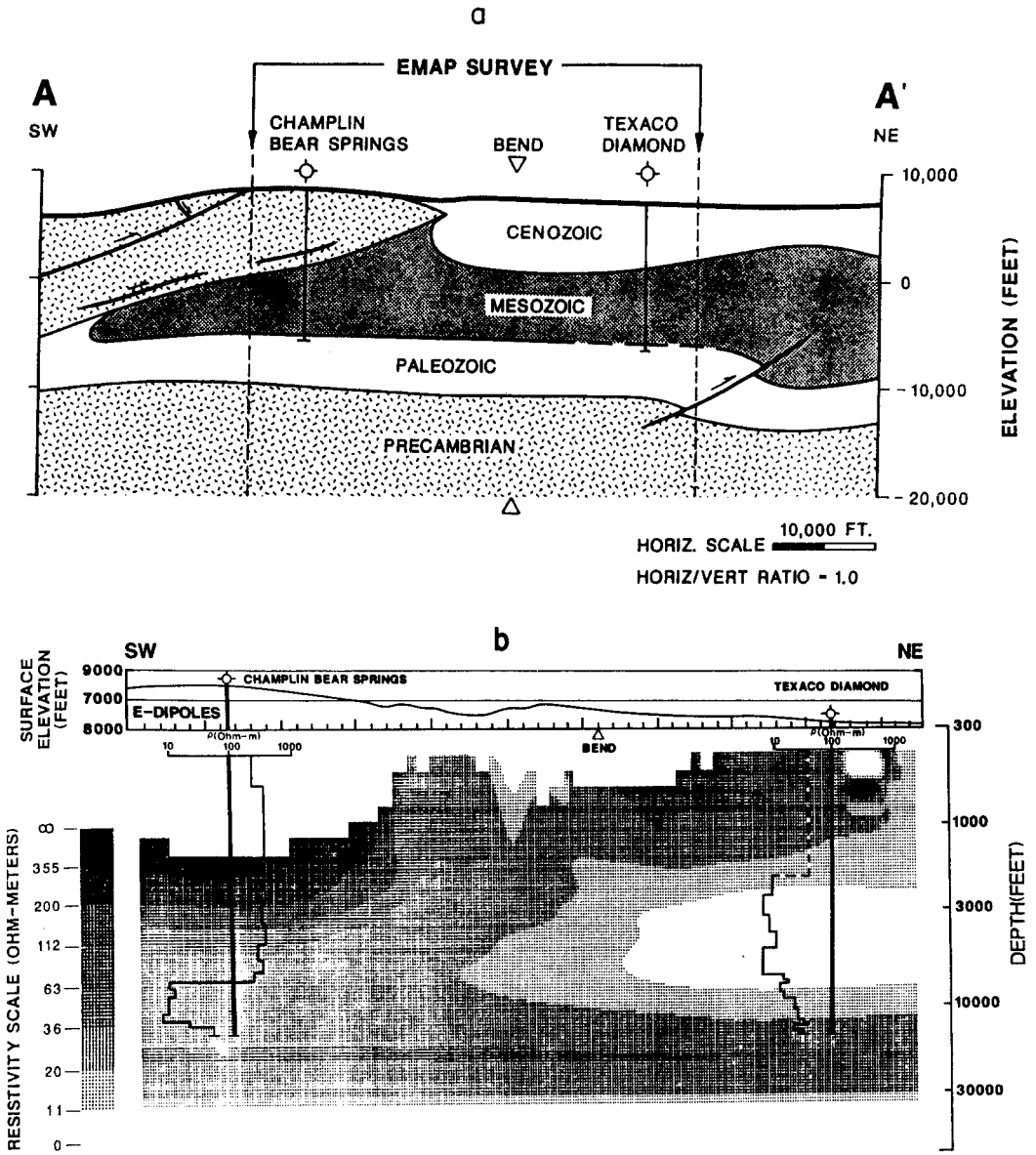


Fig. 16. EMAP applied to actual data. (a) Geological cross section along EMAP survey line in Colorado, U.S.A. (b) EMAP calculated resistivity versus depth section and comparison with borehole resistivity logs (after Word *et al.*, 1986).

A theoretical example (Figure 17) from Jiracek *et al.* (1989b) presents the results of stripping the distortion effects of 200 m high 2-D cosinusoidal topography. Figure 18 contains the real parts of TE and TM distortion tensor elements versus period at MT station 1 (Figure 17a). In the 2-D case with  $y$  the strike direction,  $D_{yy}^E$  is simply the ratio  $E_y^D/E_y^U$ ,  $D_{xx}^H$  is  $H_x^D/H_x^U$ , etc. The form of the distortion tensor

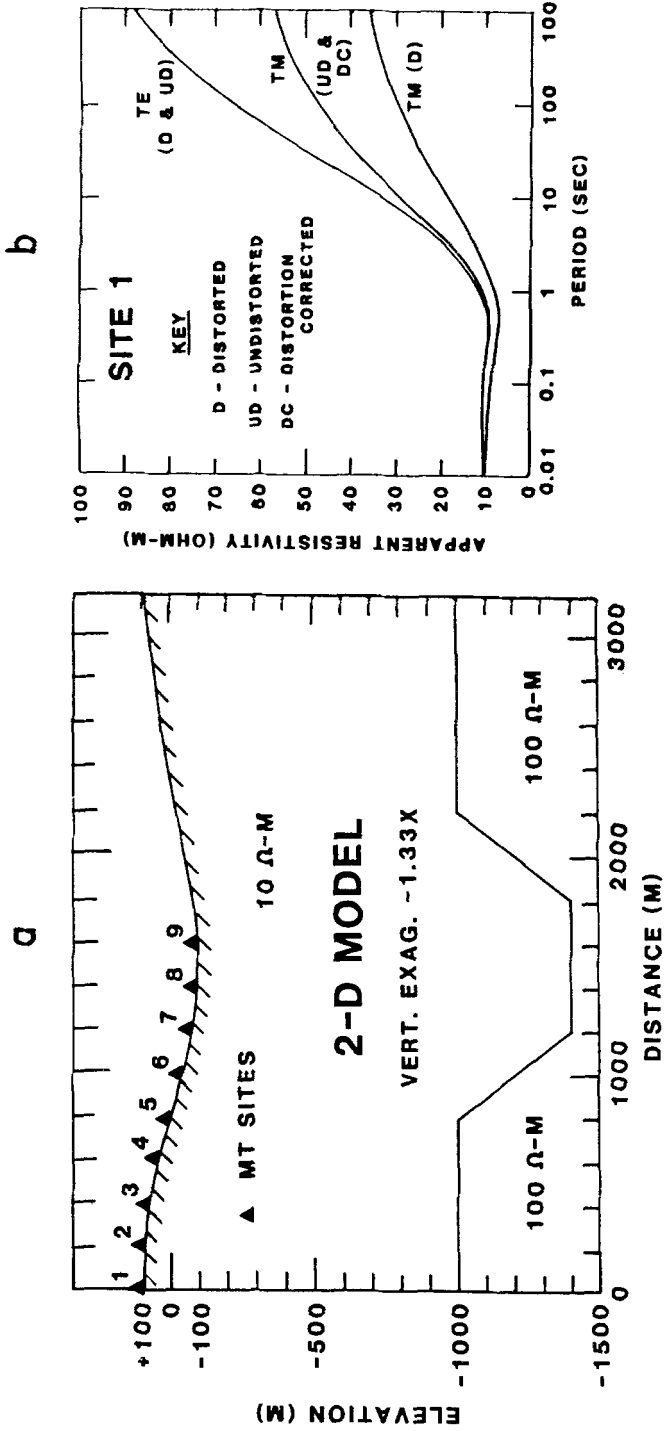


Fig. 17. Theoretical correction of distorted MT curves by distortion tensor stripping. (a) Geometry of 2-D cosinusoidal topography and horst-graben subsurface. (b) Distorted, undistorted, and distortion corrected TE and TM apparent resistivity sounding curves at site 1 of (a) (after Jiracek *et al.*, 1989b).

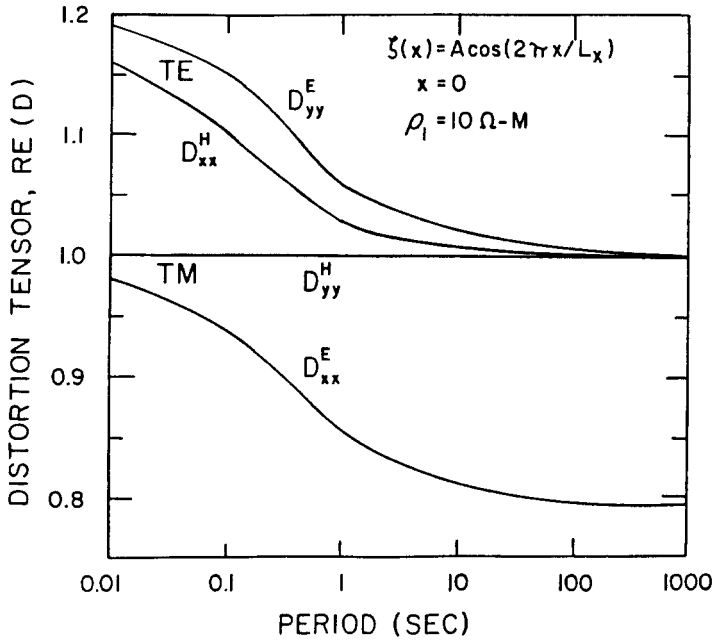


Fig. 18. Real parts of the TE and TM distortion tensor elements versus period at site 1 ( $x = 0$ ) in Figure 17a (after Jiracek *et al.*, 1989b).

curves (Figure 18) contains the essence of topographic inductive and galvanic effects. Both the electric and magnetic fields are distorted in the TE (inductive) case by amounts that decrease with increasing period. A value of 1 for the distortion tensor element means no distortion. The TE topographic distortion also approaches zero at much higher frequencies when the skin depth in the  $10 \Omega\text{-m}$  layer is much less than the topographic relief. From Figure 18 it is clear that both TE electric *and* magnetic fields are distorted by 2-D topography, but the response as manifested by the apparent resistivity (proportional to the E/H field ratio) is small. The TM electric field distortion approaches zero ( $D_{xx}^E \rightarrow 1$ ) at short periods (Figure 18); at long periods, the skin depth is greater than the surface topography and surface charges increase and saturate. This galvanic effect reaches a near constant value of distortion, therefore a static effect, above approximately 100 s period. The TM magnetic field distortion is negligible ( $D_{yy}^H = 1$ ); therefore, the TM distortion is controlled solely by the electrical field distortion as has been discussed earlier. From Figure 17b the TE distortion is obviously insignificant; however, the TM distortion produces an anomalous decrease in apparent resistivity on topographic peaks. Since TM distortion is a function of period until 100 s (Figure 18), a static shift would not correctly displace the curve until above 100 s. Applying distortion tensor stripping produces a corrected curve (DC) in agreement with the undistorted (non topographic) TM calculation (Figure 17b).

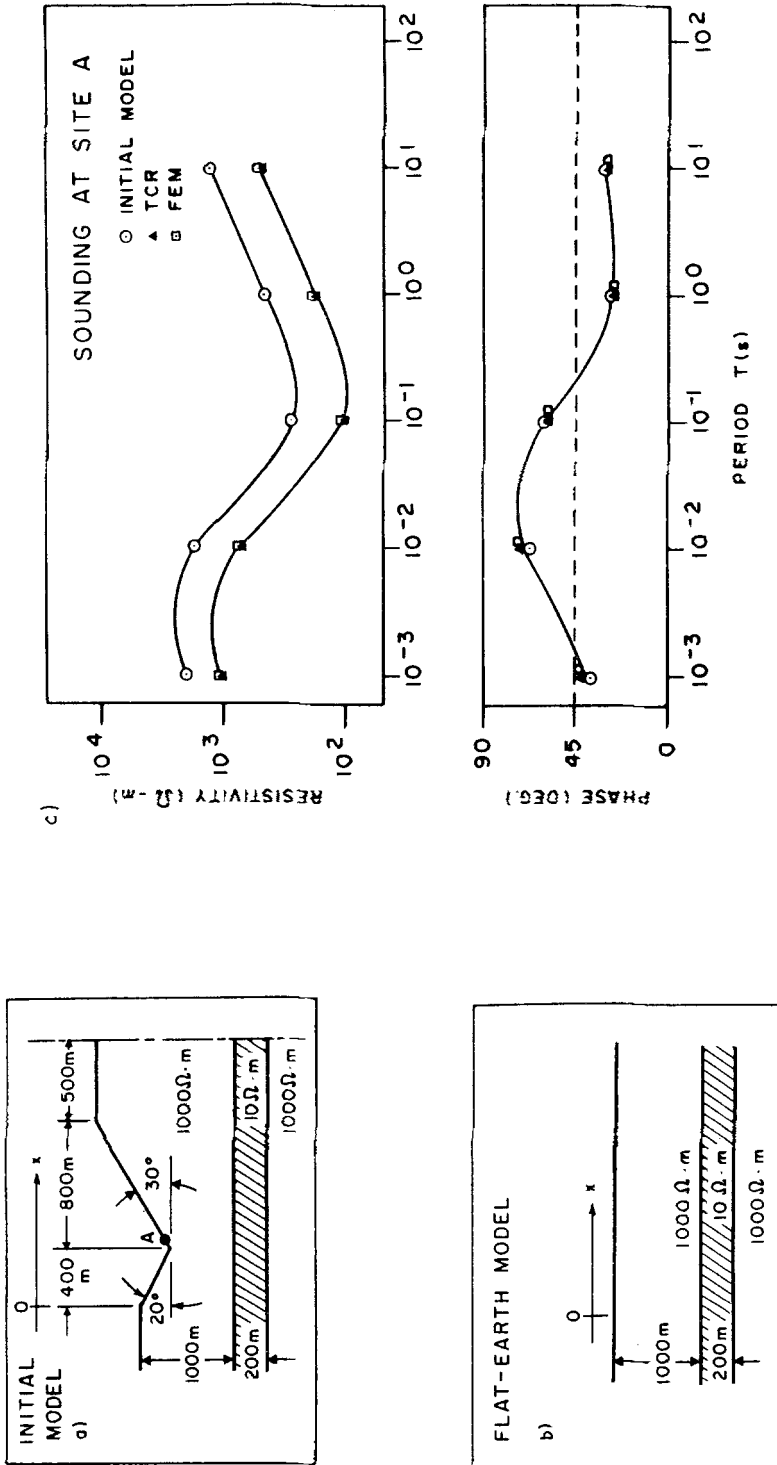


Fig. 19. Theoretical correction of distorted MT curve by distortion tensor stripping. (a) Geometry of initial model with topography over layered earth. (b) Geometry of flat-earth model. (c) Initial (distorted) model, terrain corrected (TCR), and flat earth model (FEM) TM apparent resistivity and impedance phase sounding curves at site A in (a) (after Chouteau and Bouchard, 1988).

Chouteau and Bouchard (1988) also present results of 2-D terrain correction by distortion tensor stripping. They show that subsurface structures may be distorted in the process and that the choice of the model used for the undistorted field calculation may vary with frequency. Figure 19 presents one of their earth models, the TM distorted curve in a topographic valley, and the terrain-corrected (TCR) and flat earth model (FEM) results.

Another stripping method applied in the USSR is to calculate the value of admittance reduced to the bottom of a surface sedimentary sequence (Berdichevsky *et al.*, 1989). The method requires the calculation of the integrated conductance of the sedimentary layer. This is done from the initial ascending branch of the sounding curves (the  $S_1$ -interval) and the value of integrated conductance is simply subtracted from the observed surface admittance. The reduced admittance is then used to calculate apparent resistivity curves reduced to the surface of the crystalline basement. The required approximations hold for a horizontally homogeneous model; therefore, this technique is not appropriate for small to medium scale inhomogeneities.

An example of distortion tensor stripping of actual MT field data from the EMSLAB (Electromagnetic Sounding of the Lithosphere and the Asthenosphere Beneath) project is presented in Figure 20. In this case, three conductive features (Figure 20a) – the Pacific Ocean, a thick sequence of sediments under the continental shelf, and a 2-km deep basin – were modeled and their effects removed. The distortion corrected DC results (Figure 20b) are nearly equal but 1-D modeling does not agree with more extensive 2-D modeling in the area (Jiracek *et al.*, 1989a). This casts doubt on the validity of the assumed geometry and resistivity of the distorting features. Such uncertainty is the major problem in applying distortion tensor stripping. The technique is probably more applicable to topographic stripping alone. Even in this case, however, resistivity variations should be modeled and a flat, homogeneous undistorted model may be too simplified.

Groom and Bailey (1989) have recently factored the  $2 \times 2$  distortion tensor remaining in equation 15 when  $E_z$  is zero into real matrices representing twist, rotation, and imposed anisotropy. This decomposition assumes a 1-D or 2-D regional electric field in the presence of local 3-D galvanic effects. They further decompose the measured distorted impedance tensor into the two correct complex regional impedances, the correct regional strike, and two new parameters called twist and shear. Finally, the true regional impedance elements (if 1-D or 2-D) are recovered (except for a static shift) by solving a nonlinear system of equations. The method appears to have considerable merit in removing distortion effects when the assumption that local 3-D inductively weak, galvanic distortion obscures an otherwise 1-D or 2-D regional structure is valid. Figure 21 compares the results of conventional analysis of actual MT data with the Groom-Bailey analysis. In particular it is clear, by their near coincidence, that the conventional regional strike is dominated by the azimuth of the local distortion. Also, although the conventional major and minor apparent resistivities appear to be static shifted (also evident by

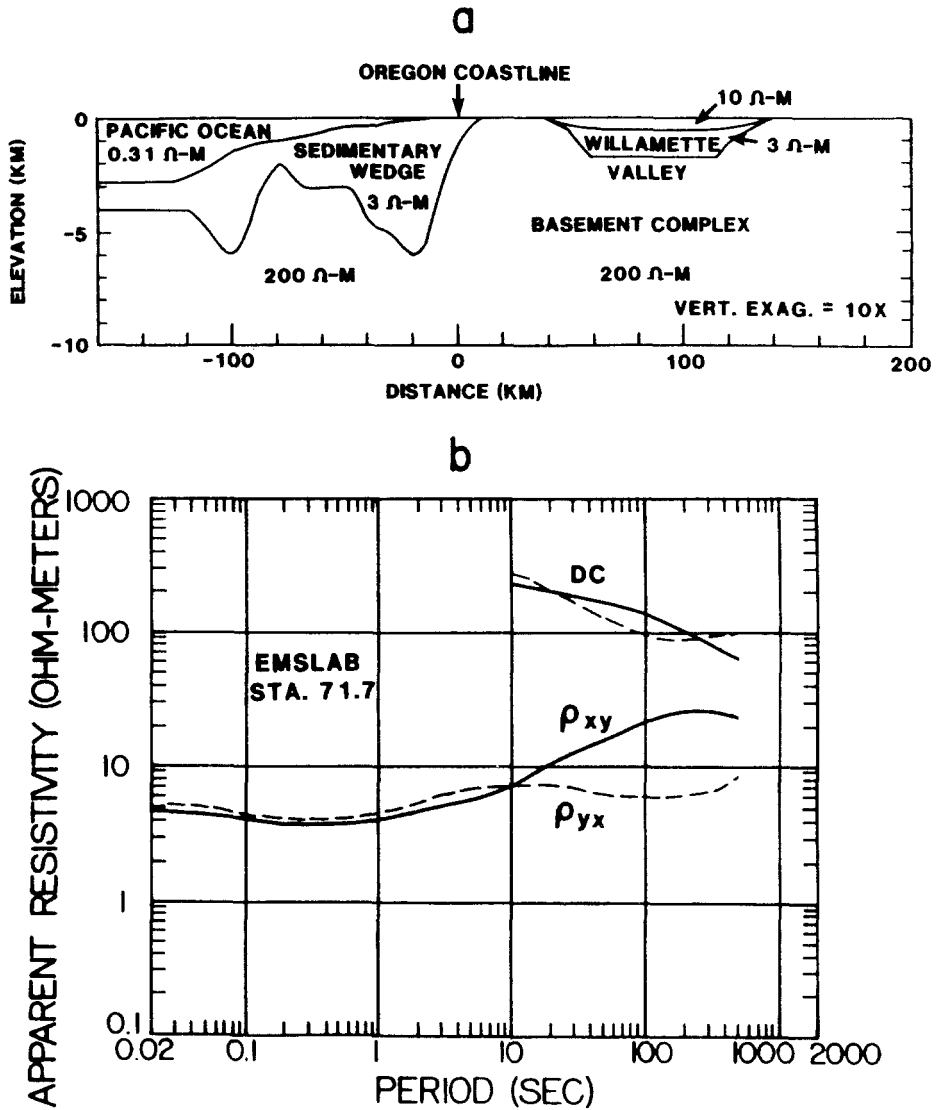


Fig. 20 Distortion tensor stripping applied to actual data. (a) Geometry of EMSLAB near-surface 2-D model. (b) Observed and distortion corrected (DC)  $\rho_{xy}$  and  $\rho_{yx}$  apparent resistivity sounding curves using model in (a) at MT site 71.7 km east of Oregon U.S.A. coastline.

the near-equality of the impedance phases), the new technique yields very different regional apparent resistivities, phases, and strike variations. Zhang *et al.* (1987) discussed similar distortions when the local structures are 2-D.

Groom and Bailey (1989) have suggested the use of their decomposition as a standard way to present real and synthetic 3-D MT data. Their seven real parameters, compared to five in the standard 2-D analysis, do provide more physical insight than the full eight parameter impedance decompositions (e.g., Eggers, 1982; La Torraca *et al.*, 1986).

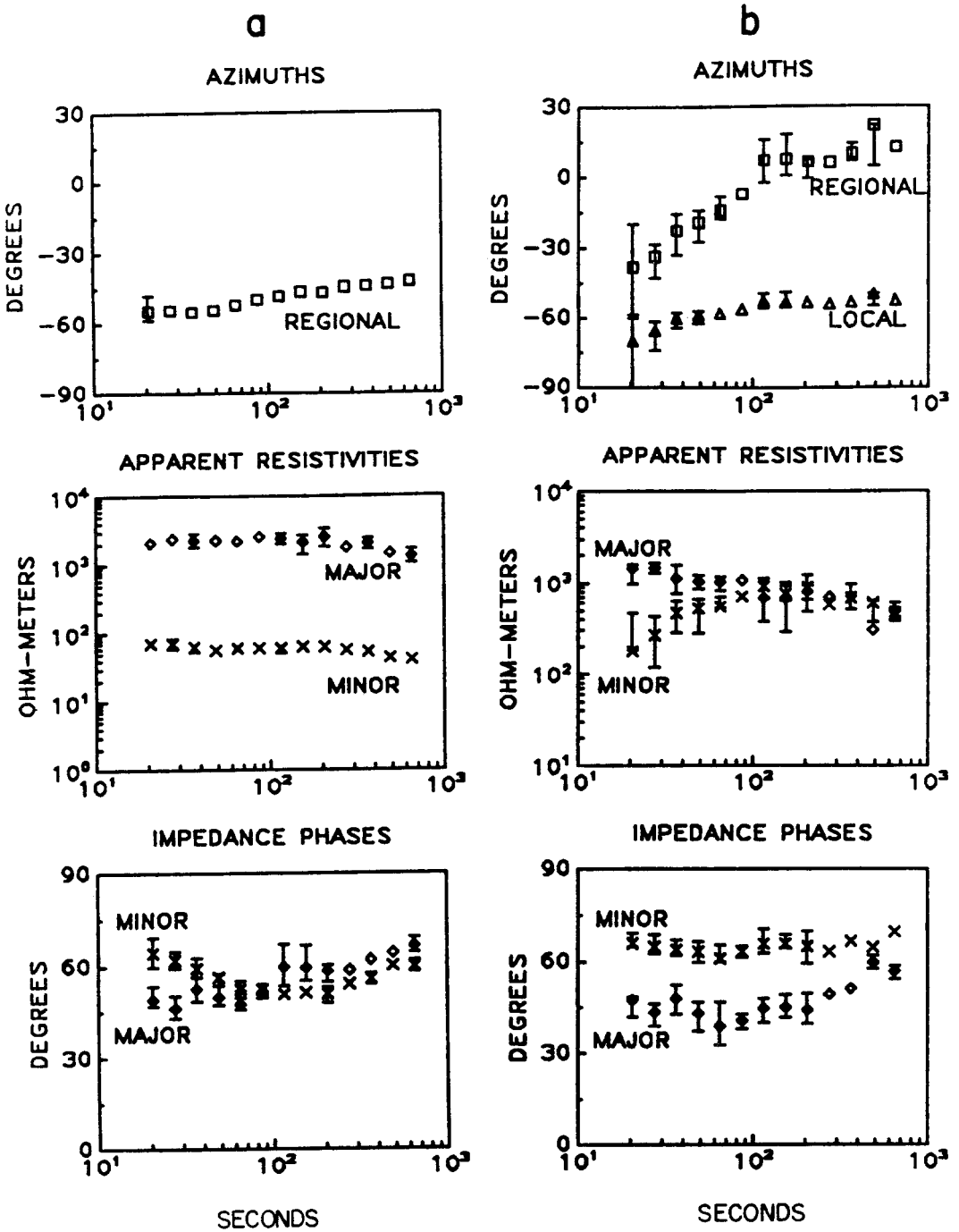


Fig. 21. Comparison of conventional and new impedance tensor decomposition. Graphs of (a) conventional and (b) new strike determinations, apparent resistivities, and impedance phases (after Groom and Bailey, 1989).

## COMPUTER MODELING

It is not within the scope of this paper to review the large array of EM modeling schemes. Several authors have presented theoretical EM results over 3-D bodies (e.g., Jones and Pascoe, 1973; Weidelt, 1975; Reddy *et al.*, 1977, Ting and Hohmann, 1981; Hermance, 1982; Park *et al.*, 1983; Wannamaker *et al.*, 1984; Park, 1985). An example of the distortion due to a 4 km thick 3-D body in an otherwise layered-earth sequence is contained in Figure 22 as reported by Park (1985). Plotted as functions of frequency, the ascending branches of both the N-S and E-W curves are distorted by more than two decades compared to the 1-D curve. Park (1985) believes that local induction is as important or more so compared to current distortion effects (galvanic effects). However, it appears that the majority of the curve shifting is due to galvanic effects in both the N-S and E-W modes. These effects are similar to those discussed regarding Figure 1 when two orthogonal orientations (N-S and E-W) of the incident electric field are considered. Over a surface 3-D conductive body, both the quasi TE (N-S) and the quasi TM (E-W) sounding curves are depressed.

Three-dimensional modeling of the variable conductance of the sedimentary cover has been very effective in evaluating the deeper section (e.g., Vanyan *et al.*, 1984; Kaikkonen *et al.*, 1985). This approach extends the earlier work of Schmucker (1971), wherein the surface layer was modeled by the so called 2-D Price

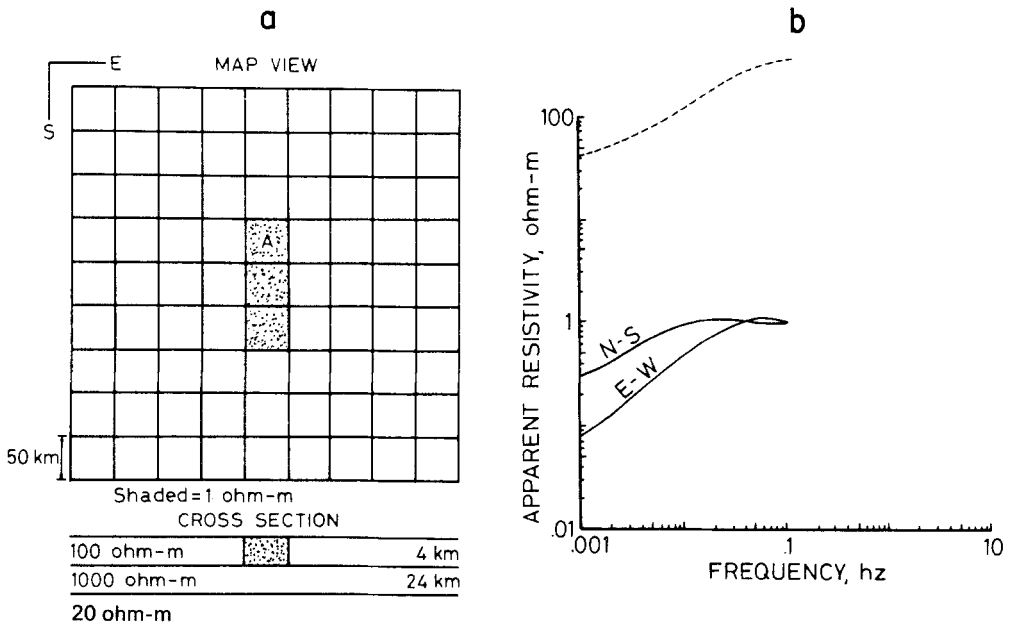


Fig. 22. Theoretical 3-D modeling. (a) Geometry of 3-D  $1 \Omega\text{-m}$ , 4 km thick surficial inhomogeneity in a layered earth. (b) N-S and E-W apparent resistivity sounding curves calculated inside  $1 \Omega\text{-m}$  conductor at site A in (a) and 1-D normal curve outside of conductor (after Park, 1986).

thin-sheet. An extension of this concept to 3-D is described in Berdichevsky and Zhdanov (1984). A generalized Price thin-sheet algorithm has been used by Park (1985), Gustafson (1986), and Park and Torres-Verdin (1988) to evaluate the 3-D effects of basin-wide distortions. Inherent in using these 3-D modeling codes is the comparison of the results with observed data. If the observed data can be explained by the calculated shallow responses then deeper structures may not be present. The 3-D modeling necessitates a knowledge of the integrated surface conductance which requires regional near-surface resistivities and thicknesses.

The 3-D modeling of Wannamaker *et al.* (1984) concluded that 2-D modeling of the mode identified as TM gives correct estimates of the true geoelectric section in many cases. This appears to be true in the vicinity of isolated blocks but Gustafson (1986) has illustrated a situation where the converse is true. The theoretical 3-D model plotted in plan view in Figure 23 is that of a prismatic basin with a narrow, connecting channel. The model consists of a 30 km wide (3 km deep) basin narrowing to 10 by 1 km cross-section in the constriction. Each segment of the basin has a resistivity of  $10 \Omega\text{-m}$ ; the host resistivity is  $500 \Omega\text{-m}$ . The 3-D  $\rho_{xy}$  and  $\rho_{yx}$  sounding curves are calculated for a station located 5 km from the mouth of the constriction. This is compared in Figure 23 with the TE and TM results if the geometry was cross-sectionally 2-D. Obviously, a 2-D TM analysis of the 3-D  $\rho_{yx}$  data would not yield proper results but a 2-D TE analysis of the 3-D  $\rho_{xy}$  would be closer.

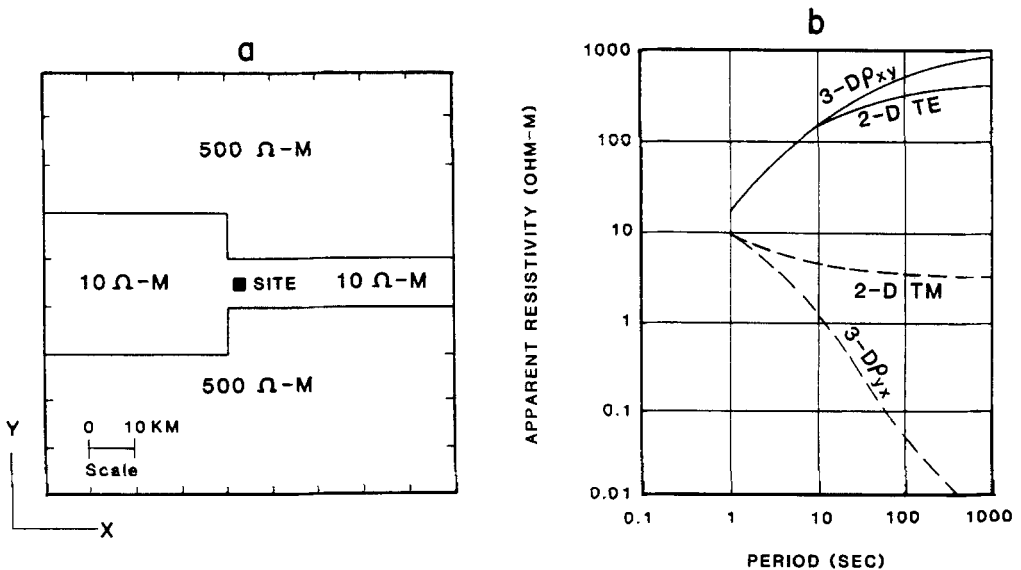


Fig. 23. Theoretical comparison of 2-D and 3-D modeling. (a) Geometry of 3-D constricted basin model in map view. Model parameters are given in text. (b) Apparent resistivity curves calculated for 3-D model ( $\rho_{xy}$  and  $\rho_{yx}$ ) and for  $y$  cross-section, 2-D model (TE and TM) at station location in (a) (after Gustafson, 1986).

For 2-D TM modeling of the 3-D situations Gamble *et al.* (1981) and Wannamaker *et al.* (1984) advocate a fixed coordinate system. It is derived using the tipper-strike calculated in a period range where the vertical  $H_z$  response from the desired deep structure is dominant. The calculations of Wannamaker *et al.* (1984) and Pellerin (1988) emphasize the superiority of the band-limited tipper definition of regional strike compared to the distorted principal directions derived from the impedance tensor. However, a fixed coordinate system may mix the quasi TE and TM modes more than station by station, period by period rotations. Hence, the answer to the question of which data are 'best' for 2-D modeling is survey

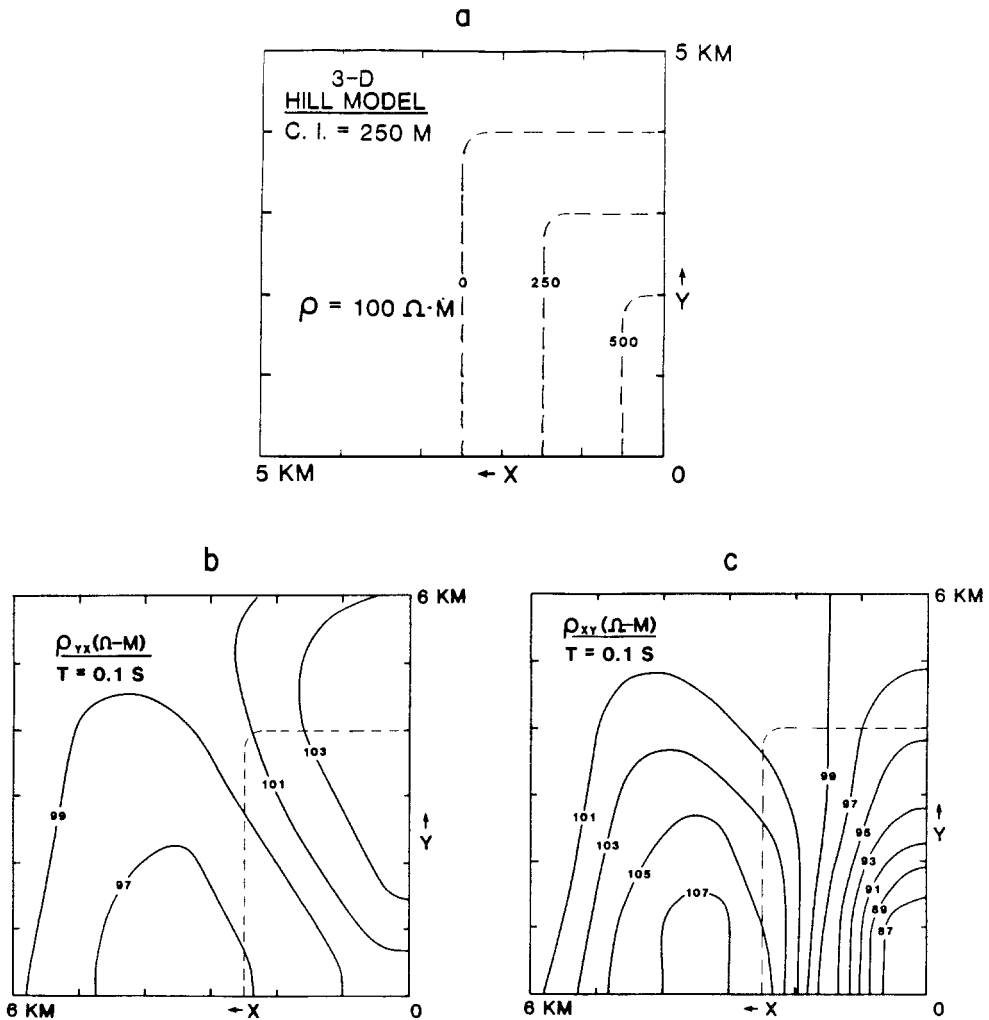


Fig. 24. Theoretical 3-D topographic modeling. (a) Geometry of 3-D cylindrically shaped 100  $\Omega$ -m hill shown by elevation contours in one quadrant. Apparent resistivity values also plotted in one quadrant at 0.1 s period for (b)  $\rho_{yx}$  and (c)  $\rho_{xy}$  (after Boersma and Jiracek, 1987).

dependent. There are instances where 2-D modeling of 3-D data can not be properly done with either fixed or a variable coordinate system.

Topographic modeling has been accomplished in 2-D by various techniques: finite difference-transmission line analogy (Ku *et al.*, 1973), conformal transformation (Thayer, 1975; Harinarayana and Sarma, 1982; Harinarayana, 1986), finite element calculations (Wannamaker *et al.*, 1986), and Rayleigh-FFT (Reddig and Jiracek, 1984; Jiracek *et al.*, 1989b). Finite difference modeling of 3-D topography appeared as early as 1976 (Ramaswamy *et al.*, 1976) and Mozley (1982) used a transmission network analogy. Boersma and Jiracek (1987) have recently calculated 3-D topographic effects using the Rayleigh-FFT method (Figure 24).

Modeling studies of 3-D inhomogeneities and topography provide important insight into actual situations. In fact, Fainberg and Singer (1987) believe that the "determinations of anomalous field values can, with few exceptions, be solved *only* with the help of modelling". This follows exactly the sentiment of Park and Torres-Verdin (1986) who state that "3-D modeling simply cannot be avoided in complex geological environments".

### Conclusions

It is difficult to make firm conclusions on how best to handle the distortions due to surficial inhomogeneities and topography in EM soundings. A recommended procedure must consider the entire data collection and modeling process. In this sense, one must address the complete spectrum from the ideal (unattainable) to the most practical.

Probably the ideal data set would be areal EMAP coverage which included effective electric field dipole lengths from tens of meters to many kilometers. Even with such a 2-D array there would probably be distorting features outside of the survey area whose adjustment distances include the array. One must seriously evaluate the EMAP concept of continuous profiling in the light of spatial aliasing. Via the sampling theorem, there must be at least two samples per spatial wavelength to obtain information about features of comparable size. If small features are not present in the study area then continuous dipoles are not necessary. If their spectral energy is slight, little aliased information is folded back at the spatial Nyquist frequency provided the dipole lengths are calculated to provide sufficient antialias protection. The spatial 1-D or 2-D filtering of EMAP (or conventional MT data) could profit from filter responses designed for specific purposes, e.g., the removal of known topography or known basin configuration. The present EMAP filter response is that of a Hanning window. The final step in the EMAP process, namely modeling of the filtered data, can surely profit from 2-D and 3-D forward and inverse modeling rather than a 1-D interpretation. Commercial EMAP data collection may soon rival seismic reflection data acquisition in quantity; therefore, better, more efficient ways of handling large volumes of MT data must be forthcoming.

The practical removal of the unwanted surficial EM distortions has been characterized in this review by six categories, some not totally distinct. The most attractive approaches developed by MT practitioners integrate several methods into an overall scheme, e.g., the MTFDI scheme of Reddig *et al.* (1989), the space analysis described by Zhdanov (1987), and the systematic approach of Park and Torres-Verdin (1988). One is usually faced with the removal of inherently different effects: (1) topography, (2) near-station inhomogeneities, and (3) regional distortion. The averaging or filtering of data from neighboring stations having conformal but shifted apparent resistivity curves has proven very useful when the first two effects are random. This requires many soundings. Here, the retention of tensor data rather than effective impedances is recommended. The shifting of sounding curves can be accomplished using auxiliary information such as TEM soundings or well logs but another survey must be run. However, the requirement of excessive data may be forestalled if the new distortion model and tensor decomposition of Groom and Bailey (1989) is applicable. Synthetic 3-D tests of this procedure should be made to evaluate its value in removing EM distortion and in routine data representation.

The need for 3-D modeling is not lessened under any circumstances since: (1) the removal of 3-D topographic effects is possible via tensor stripping since the geometry can be obtained, (2) regional 3-D effects (point 3 above) must be evaluated for large-scale surroundings whether or not the new tensor decomposition is used, (3) distortion removal schemes should always be evaluated theoretically in 3-D to test their applicability and, (4) most EM targets are really 3-D at the scale lengths that are sensed whether near-surface effects are removed or not.

Ultimately one probably needs to try different EM distortion schemes either alone or in conjunction with each other. No one method is a panacea and the user must be wary of their effects on the data so as not to be misled. The simplest correction techniques are best only if they *are* correct: the complex nature of EM distortions may not permit simple solutions.

### Acknowledgements

To a large degree this review has been an exercise in compilation rather than research. In either case I have benefited enormously from an enthusiastic response from colleagues world-wide who answered my call for pertinent work. They have all my deepest appreciation. I hope that they will forgive my shortcomings if I have misquoted them or have not used their contributions. It was difficult to keep this review to a manageable size. To my friends and colleagues Jerry Hohmann, Frank Morrison, and Mario Martinez I owe a special thanks for their reviews of the manuscript. They and an anonymous reviewer have helped greatly to improve the paper; however; they do not share the responsibility for any remaining deficiencies.

## References

- Adam, A., Szarka, L., Vero, J., and Wallner, A.: 1986, 'Magnetotellurics (MT) in Mountains – Noise, Topography and Crustal Inhomogeneity Effects', *Phys. Earth Planet. Inter.* **42**, 165–177.
- Andrieux, P. and Wightman, W. E.: 1984, 'The So-called Static Correction in Magnetotelluric Measurements', 54th Ann. Internat. Mtg., Soc. Explor. Geophys., Expanded Abstracts, pp. 43–44.
- Berdichevsky, M. N., Bezruk, I. A., and Chinavera, O. M.: 1973, 'Magnetotelluric Sounding with the Use of Mathematical Filters (in Russian)', *Izv. Akad. Nauk SSSR Fiz. Zeml.* **3**, 72–92.
- Berdichevsky, M. N. and Dmitriev, V. I.: 1976a, 'Distortion of Magnetic and Electric Fields by Near-Surface Lateral Inhomogeneities (in Russian)', *Acta Geod., Geophys. Mont. Hung.* **11**, 447–483.
- Berdichevsky, M. N. and Dmitriev, V. I.: 1976b, 'Basic Principles of Interpretation of Magnetotelluric Sounding Curves', in Adam, A. (ed), *Geoelectric and Geothermal Studies*, KAPG Geophysical Monograph, Akademiai Kiado, pp. 165–221.
- Berdichevsky, M. N., Vanyan, L. L., Kuznetsov, V. A., Levadny, V. T., and Mandelbaum, M. M., Nechaeva, G. P., Okulesky, B. A., Shilosky, P. P., and Shpak, I. P.: 1980, 'Geoelectrical Model of the Baikal Region', *Phys. Earth Planet. Inter.* **22**, 1–11.
- Berdichevsky, M. N. and Zhdanov, M. S.: 1984, *Advanced Theory of Deep Geomagnetic Sounding*, Elsevier Sci. Pub., Amsterdam, 408 pp.
- Berdichevsky, M. N., Vanyan L. L., and Dmitriev, V. I.: 1989, 'Methods Used in the U.S.S.R. to Reduce Near-Surface Inhomogeneity Effects on Deep Magnetotelluric Sounding', *Phys. Earth Planet. Inter.* **53**, 194–206.
- Boersma, J. R. and Jiracek, G. R.: 1987, 'Three-Dimensional Magnetotelluric Modelling with the Rayleigh-FFT Method', *Internat. Union of Geodesy and Geophysics General Assembly, Vancouver, Canada, Abs.* **2**, 1452.
- Bostick, F. X. Jr.: 1977, 'A Simple Almost Exact Method of MT Analysis', in Ward, S. (ed.), *Workshop on Electrical Methods in Geothermal Exploration*, Univ. of Utah Res. Inst., U.S. Geol. Surv. Contract 14-08-0001-g-359, pp. 174–183.
- Bostick, F. X. Jr.: 1986, *Electromagnetic Array Profiling (EMAP)*: 56th Ann. Internat. Mtg., Soc. Explor. Geophys., Expanded Abstracts, 60–61.
- Chouteau, M and Bouchard, K.: 1988, 'Two-Dimensional Terrain Correction in Magnetotelluric Surveys', *Geophysics* **6**, 854–862.
- Dawson, T. W., Weaver, J. T., and Raval, V.: 1982, 'B-polarization Induction in Two Generalized Thin Sheets at the Surface of a Conducting Half-Space', *Geophys. J. R. Astr. Soc.* **69**, 209–234.
- Dmitriev, V. I., Zakharov, E. V., and Kokotushkin, G. A.: 1973, *Master Curves for Magnetotelluric Sounding in Homogeneous Media (in Russian)*. **2**, Moscow State Univ.
- Dosso, H. W. and Weaver, J. T.: 1983, 'The Collective Review Papers Presented at the 6th IAGA Workshop on Electromagnetic Induction in Earth and Moon-Preface', *Geophys. Surv.* **6**, 103.
- Eggers, D. E.: 1982, 'An Eigenstate Formulation of the Magnetotelluric Impedance Tensor', *Geophysics* **47**, 1204–1214.
- Fainberg, E. B. and Singer, B. Sh.: 1987, 'The Influence of Surface Inhomogeneities on Deep Electromagnetic Soundings of the Earth', *Geophys. J. R. Astr. Soc.* **90**, 61–73.
- Fischer, G. and Le Quang, B. V.: 1981, 'Topography and Minimization of the Standard Deviations in One-Dimensional Magnetotelluric Modelling', *Geophys. J. R. Astr. Soc.* **67**, 279–292.
- Fischer, G. and Weaver J. T.: 1986, 'Theoretical Investigation of the Ocean-Coast Effect at a Passive Continental Margin', *Phys. Earth Planet. Inter.* **42**, 246–254.
- Fuller, B. D.: 1967, 'Two-Dimensional Frequency Analysis and Design of Grid Operators: in *Mining Geophysics*, v. 2, Soc. Expl. Geophys. 658–703.
- Gamble, T. D., Goubau, W. M., Goldstein, N. W., Miracky, R., Stark, M., and Clarke, J.: 1981, 'Magnetotelluric Studies at Cerro Prieto', *Geothermics* **10**, 169–182.
- Gomez-Trevino, E.: 1987, 'Should the Electric Line be Straight in Magnetotelluric Surveys?', *Geophys. Prosp.* **35**, 920–923.
- Groom, R. W. and Bailey, R. C.: 1989, 'Decomposition of Magnetotelluric Impedance Tensors in the Presence of Local Three-Dimensional Galvanic Distortion', *J. Geophys. Res.* **94**, 1913–1925.
- Gustafson, E. P.: 1986, 'Three-Dimensional Magnetotelluric Response of the Rio Grande Rift near Socorro, New Mexico', M.S. Thesis, San Diego State Univ.

- Harinarayana, T.: 1986, *Distortion of Telluric Field Measurements near a Hill*, 8th Workshop on Electromagnetic Induction in the Earth and Moon, Neuchâtel, Switzerland, abs., pp. 7–1.
- Harinarayana, T. and Sarma, S. V. S.: 1982, 'Topographic Effects on Telluric Field Measurements', *Pure Appl. Geophys.* **120**, 778–783.
- Hermance, J. F.: 1982, 'The Asymptotic Response of Three-Dimensional Basin Offsets to Magnetotelluric Fields at Long Periods: The Effects of Current Channeling', *Geophysics* **47**, 1562–1573.
- Hohmann, G. W.: 1988, 'Numerical Modeling for Electromagnetic Methods of Geophysics', in Nabighian, M. N., (ed.), *Electromagnetic Methods in Applied Geophysics – Theory*, v.1., Soc. Explor. Geophys., Tulsa, pp. 313–363.
- Honkura, Y.: 1983, 'Peninsular Effects in Central Japan and Their Relation to the Electrical Conductivity Structure', *J. Geomag. Geoelectr.* **35**, 39–56.
- Honkura, Y.: 1987, 'Elimination of the Regional Coast Effect and a Local Resistivity Structure in the Norboribetsu Geothermal Area, Southwestern Hokkaido', *J. Geomag. Geoelectr.* **39**, 751–767.
- Honkura, Y., Isezaki, N., and Yaskawa, K.: 1981, 'Electrical Conductivity Structure Beneath the Northwestern Philippines Sea as Inferred from the Island Effect on Minami-Diato Island', *J. Geomag. Geoelectr.* **33**, 365–377.
- Jensen, V and Seara, J. L.: 1988, *Case History: The ECRE Method Applied to a Two-Dimensional Salt Structure*, Geometra Ltd., 16 pp.
- Jiracek, G. R., Gustafson, E., and Mitchell, P. S.: 1983, 'Magnetotelluric Results Opposing Magma Origin of Crustal Conductors in the Rio Grande Rift', *Tectonophysics* **94**, 299–326.
- Jiracek, G. R., Curtis, J. H., Ramirez, J., Martinez, M., and Romo, J.: 1989a, 'Two-Dimensional Magnetotelluric Inversion of the EMSLAB Lincoln Line', *J. Geophys. Res.* **94**, 14,145–14,151.
- Jiracek, G. R., Reddig, R. P., and Kojima, R. K.: 1989b, 'Application of the Rayleigh-FFT Technique to Magnetotelluric Modelling and Correction', *Phys. Earth Planet. Inter.* **53**, 365–375.
- Jones, A. G.: 1983, 'The Problem of Current Channelling: A Critical Review', *Geophys. Surv.* **6**, 79–122.
- Jones, A. G.: 1986, 'On the Use of Line Current Analogues in Geomagnetic Depth Sounding', *J. Geophys.* **60**, 56–62.
- Jones, A. G.: 1988, 'Static-Shift of Magnetotelluric Data and its Removal in a Sedimentary Basin Environment', *Geophysics* **7**, 967–978.
- Jones, F. W. and Pascoe, L. J.: 1973, 'The Perturbations of Alternating Geomagnetic Fields by Three-Dimensional Structures', *Geophys. J. R. Astr. Soc.* **32**, 133–154.
- Jones, F. W. and Price, A. T.: 1970, 'The Perturbations of Alternating Geomagnetic Fields by Conducting Anomalies', *Geophys. J. R. Astr. Soc.* **20**, 317–334.
- Kaikkonen, P., Vanyan, L. L., Martanus, E. R., and Okulesky, B. A.: 1985, 'Contribution of the Surficial Effects on the Low-frequency Magnetotelluric Anomaly at the Rheingraben Area', *Phys. Earth Planet. Inter.* **37**, 223–227.
- Kaufmann, A. A.: 1985, 'Tutorial: Distribution of Alternating Electrical Charges in a Conducting Medium', *Geophys. Prosp.* **33**, 171–184.
- Ku, C. C., Hsieh, M. S., and Lim, S. H.: 1973, 'The Topographic Effect in Electromagnetic Fields', *Can. J. Earth. Sci.* **10**, 645–656.
- Kurtz, R. D., DeLaurier, J. M., and Gupta, J. C.: 1986, 'A Magnetotelluric Sounding across Vancouver Island Detects the Subducting Juan de Fuca Plate', *Nature* **321**, 596–599.
- Lajoie, J. J. and West, G. F.: 1976, 'The Electromagnetic Response of a Conductive Inhomogeneity in a Layered Earth', *Geophysics* **41**, 1133–1156.
- Larsen, J. C.: 1977, 'Removal of Local Surface Conductivity Effects from low Frequency Mantle Response Curves', *Acta Geodaet. Geophys. et Montanist. Acad. Sci. Hung.* **12**, 183–186.
- LaTorraca, G. A., Madden R. T., and Korringa, J.: 1986, 'An Analysis of the Magnetotelluric Impedance for Three-Dimensional Conductivity Structures', *Geophysics* **51**, 1819–1829.
- Livelybrooks, D. W.: 1986, 'Modelling Earth Resistivity Structure for MT Data: A Comparison of Rotationally-Invariant and Conventional Earth Response Functions (abs.) *EOS Trans. Amer. Geophys. Union* **67**, 918.
- McNeill, J. D., 1985, 'The Galvanic Current Component in Electromagnetic Surveys, Geonics Ltd., Tech. Note TN 17, 22 p.
- Menvielle, M.: 1988, 'Effects of Crustal Conductivity Heterogeneities on the Electromagnetic Field', *Surveys in Geophysics* **9**, 319–348.

- Mikhlin, L. P.: 1984, 'MT-sounding Curves for a Five-Layer Model with a Surface Elliptical Inclusion (in Russian)', *Fiz. Zemli*, **3**, 77–80.
- Morrison, H. F., Dolan, W., and Dey, A.: 1976, 'Earth Conductivity Determinations Employing a Single Superconducting Coil', *Geophysics* **41**, 1184–1206.
- Mozley, E. C.: 1982, 'An Investigation of the Conductivity Distribution in the Vicinity of a Cascade Volcano', Ph.D. Thesis, University of California, Berkeley, LBL-15671.
- Nienaber, W., Dosso, H. W., Law, L. K., Jones, F. W., and Ramaswamy, V.: 1976, 'An Analogue Model Study of Electromagnetic Induction for Island-Continent Ocean Channels', *Phys. Earth Planet. Inter.* **13**, 169–183.
- Park, S. K.: 1985, 'Distortion of Magnetotelluric Sounding Curves by Three-Dimensional Structures', *Geophysics* **50**, 785–797.
- Park, S. K., Orange, A. S., and Madden, T. R.: 1983, 'Effects of Three-Dimensional Structure on Magnetotelluric Sounding Curves', *Geophysics* **48**, 1402–1405.
- Park, S. K. and Torres-Verdin, C.: 1988, 'A Systematic Approach to the Interpretation of Magnetotelluric Data in Volcanic Environments with Applications to the Quest for Magma in Long Valley, California', *J. Geophys. Res.* **93**, 13,265–13,283.
- Parkinson, W. D. and Jones, F. W.: 1979, 'The Geomagnetic Coast Effect', *Rev. Geophys. Space Phys.* **17**, 1999–2015.
- Pellerin, L.: 1988, 'Use of Transient Electromagnetic Soundings to Correct Static Shifts in Magnetotelluric Data', M.S. Thesis, Univ. Utah.
- Poll, H. E., Weaver, J. T., and Jones, A. G.: 1989, 'Calculations of Voltages for Magnetotelluric Modelling of a Region with Near-Surface Inhomogeneities', *Phys. Earth Planet. Inter.* **53**, 287–297.
- Price, A. T.: 1973, 'The Theory of Geomagnetic Induction', *Phys. Earth Planet. Inter.* **7**, 227–233.
- Price, A. T. and Jones, F. W.: 1972, 'Reply by Authors to Discussion by John F. Hermance', *Geophysics* **37**, 541–542.
- Ramaswamy, V., Jones, F. W., and Dosso, H. W.: 1976, 'A Numerical Study of the Topographic Effect on Electromagnetic Fields in a Three-Dimensional Conductivity Model', *Pure Appl. Geophys.* **114**, 653–662.
- Ranganayaki, R. P. and Madden T. R.: 1980, 'Generalized Thin Sheet Analysis in Magnetotellurics: An Extension of Price's Analysis', *Geophys. J. R. Astr. Soc.* **60**, 445–457.
- Reddig, R. P. and Jiracek, G. R.: 1984, *Topographic Modeling and Correction in Magnetotellurics*, 54th Ann. Internat. Mtg., Soc. Explor. Geophys., Expanded Abstracts, pp. 44–47.
- Reddig, R. P., Holcombe, H. T. and Christopherson, K.: 1989, 'Imaging, Inversion and Modeling of Magnetotelluric Data Profiles in Wannamaker, P. E. (ed.), *Soc. Explor. Geophys. publication, Magnetotellurics in Geophysical Exploration* (submitted).
- Reddy, I. K., Rankin, D., and Phillips, R. J.: 1977, 'Three-Dimensional Modelling in Magnetotelluric and Magnetic Variational Sounding', *Geophys. J. R. Astr. Soc.* **51**, 313–325.
- Rokityansky, I. I.: 1982, *Goelectric Investigation of the Earth's Crust and Mantle*, Springer-Verlag, Berlin, 381 pp.
- Schmucker, U.: 1970, *Anomalies of Geomagnetic Variations in the Southwestern United States*, Bull. Scripps Inst. Oceanogr., Univ. of Calif. Press **13**, 165 pp.
- Schmucker, U.: 1971, 'Interpretation of Induction Anomalies Above Non-Uniform Surface Layers', *Geophysics* **36**, 156–165.
- Spies, B. R. and Frischknecht, F. C.: 1989, 'Electromagnetic Sounding', in Nabighian, M. N. (ed.), *Electromagnetic Methods in Applied Geophysics*, v.2, Soc. Explor. Geophys. (in press).
- Sternberg, B. K., Washburne, J. C., and Anderson, R. G.: 1985, *Investigation of MT Static Shift Correction Methods*, 55th Ann. Internat. Mtg., Soc. Explor. Geophys., Expanded Abstracts, pp. 264–267.
- Sternberg, B. K., Washburne, J. C., and Pellerin, L.: 1988, 'Correction for the Static Shift in Magnetotellurics Using Transient Electromagnetic Soundings', *Geophysics* **53**, 1459–1468.
- Thayer, R. E.: 1975, 'Topographic Distortion of Telluric Currents: A Simple Calculation', *Geophysics* **40**, 91–95.
- Ting, S. C. and Hohmann, G. W.: 1981, 'Integral Equation Modeling of Three-Dimensional Magnetotelluric Response', *Geophysics* **46**, 182–197.

- Torres-Verdin, C.: 1985, 'Implications of the Born Approximation for the MT Problem in Three-Dimensional Environments', M.S. Thesis, Univ. of Texas.
- Torres-Verdin, C. and Bostick, F. X., Jr.: 1989, 'Principles of Spatial Surface Electric Field Filtering in Magnetotellurics: Electromagnetic Array Profiling (EMAP)', *Geophysics* (submitted).
- Vanyan, L. L.: 1959, 'Some Problems of the Theory on the Frequency Soundings of Horizontal Stratifications (in Russian)', *Prikladnaja Geofizika* **23**, 3–45.
- Vanyan, L. L.: 1965, *Fundamentals of Electromagnetic Sounding (in Russian)*, Nedra, Moscow, 109 pp.
- Vanyan, L. L., Debabov, A. S., and Judin, M. N.: 1984, *Interpretation of Magnetotelluric Data in Inhomogeneous Media*, Nedra, Moscow, 195 pp.
- Wannamaker, P. E., Hohmann, G. W., and Ward, S. H.: 1984, 'Magnetotelluric Responses of Three-Dimensional Bodies in Layered Earths', *Geophysics* **49**, 1517–1533.
- Wannamaker, P. E., Stodt, J. A., and Rijo, L.: 1986, 'Two-Dimensional Topographic Responses in Magnetotellurics Modeled Using Finite Elements', *Geophysics* **51**, 2131–2144.
- Ward, S. H.: 1967, 'Electromagnetic Theory for Geophysical Application', in *Mining Geophysics*, v. 2, Soc. Explor. Geophys., pp. 10–196.
- Weidelt, P.: 1975, 'Electromagnetic Induction in Three-Dimensional Structures', *J. Geophys* **41**, 85–109.
- Wolfgang, P. and Scharberth, J.: 1986, *Electrical Conductivity Reference Exploration (ECRE)*, Geometra Ltd., 18 pp.
- Word, D. R., Goss, R., and Chambers, D. M.: 1986, *An EMAP Case Study*. 56th Ann. Internat. Mtg., Soc. Explor. Geophys., Expanded Abstracts, 61–63.
- Wright, J. L.: 1988, *VLF Interpretation Manual*, EDA Instruments Inc., 87 pp.
- Zhang, P., Roberts, R. G., and Pedersen, L. B.: 1986, 'Magnetotelluric Strike Rules', *Geophysics* **52**, 267–278.
- Zhdanov, M. S.: 1987, 'Application of Space Analysis of Electromagnetic Fields to Investigation of the Geoelectrical Structure of the Earth', *Phys. App. Geophys.* **125**, 483–497.